

Armed Services Technical Information Agency

Because of our limited supply, you are requested to return this copy WHEN IT HAS SERVED YOUR PURPOSE so that it may be made available to other requesters. Your cooperation will be appreciated.

AD

28598

NOTICE: WHEN GOVERNMENT OR OTHER DRAWINGS, SPECIFICATIONS OR OTHER DATA ARE USED FOR ANY PURPOSE OTHER THAN IN CONNECTION WITH A DEFINITELY RELATED GOVERNMENT PROCUREMENT OPERATION, THE U. S. GOVERNMENT THEREBY INCURS NO RESPONSIBILITY, NOR ANY OBLIGATION WHATSOEVER; AND THE FACT THAT THE GOVERNMENT MAY HAVE FORMULATED, FURNISHED, OR IN ANY WAY SUPPLIED THE SAID DRAWINGS, SPECIFICATIONS, OR OTHER DATA IS NOT TO BE REGARDED BY IMPLICATION OR OTHERWISE AS IN ANY MANNER LICENSING THE HOLDER OR ANY OTHER PERSON OR CORPORATION, OR CONVEYING ANY RIGHTS OR PERMISSION TO MANUFACTURE, USE OR SELL ANY PATENTED INVENTION THAT MAY IN ANY WAY BE RELATED THERETO.

Reproduced by
DOCUMENT SERVICE CENTER
KNOTT BUILDING, DAYTON, 2, OHIO

UNCLASSIFIED

SMI

AD N.S. 28-588

AST in FILE CUP

Semi Annual Report
of the work of the
Bartol Research Foundation of The
Franklin Institute
performed under Contract Nonr436(00)
July 1 -- December 31, 1953

SEMI ANNUAL REPORT
of the Work of the
BARTOL RESEARCH FOUNDATION
OF THE FRANKLIN INSTITUTE

(July 1, 1953 -- December 31, 1953)

Performed Under Contract No. 436(00)
with the
OFFICE OF NAVAL RESEARCH

TABLE OF CONTENTS

- I. Inelastic Scattering.
- II. Total Cross Sections; Angular Distribution
of Elastic Scattering; Inelastic Cross
Sections.
- III. Low Voltage Accelerator.
- IV. Abstract of Study of the Reactions
 $Ba^{137}(n,n')^* Ba^{137}$ and $Hg^{199}(n,n')^* Hg^{199}$.
- V. Recent Publications.
- VI. Distribution List.

PERSONNEL

Physicists: (Part-time or full-time)

D. W. Kent
C. E. Mandeville
F. R. Metzger
M. A. Rothman
S. C. Snowdon
C. P. Swann *
W. D. Whitehead **

Technicians: (Half-time)

R. W. Gunnett

* Mr. Swann has participated in this contract to the extent of coauthorship of the measurements described in Section IV. However, no part of his salary is charged to the contract.

** Terminated.

Report submitted: February 15, 1954

C. E. Mandeville
C. E. Mandeville
Assistant Director

I. INELASTIC SCATTERING.

A. Introduction.

In the previous semi-annual report incorrectly dated February 1, 1953 - June 30, 1953 (it should have been designated as January 1, 1953 - June 30, 1953) experiments falling in two different categories were described. The first group of measurements concerned themselves for the most part with a study of gamma rays excited in the nuclei of various elements by the inelastic scattering of neutrons of energy about 3.9 Mev. The remainder of the report dealt with elastic scattering of neutrons of about the same energy in aluminum, iron, and lead. From the elastic scattering data certain aspects of the inelastic scattering process are inferred.

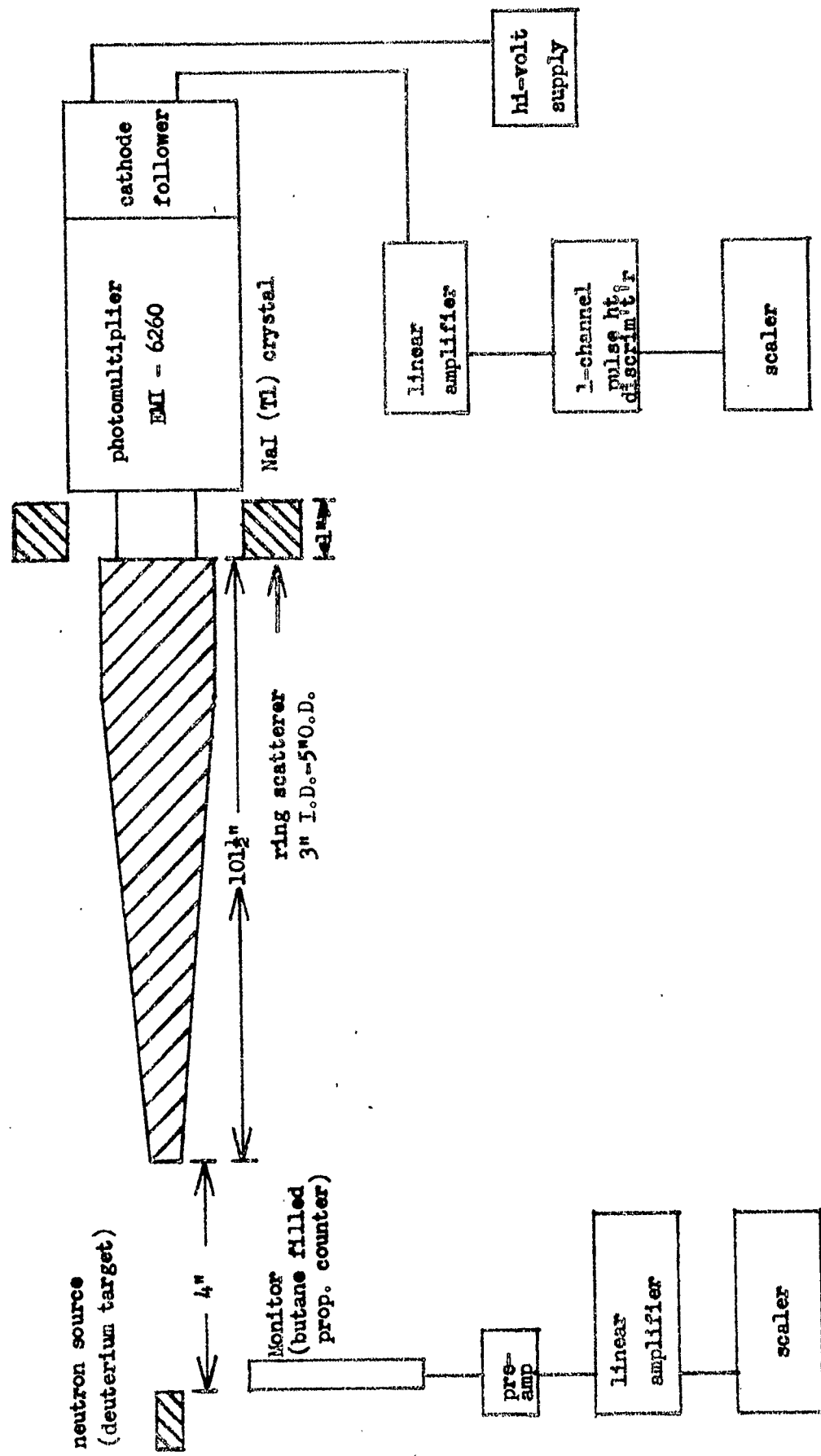
In the six months following the above mentioned report, additional results dealing with the previously discussed measurements have been obtained. The smaller Bartol Van de Graaff generator has served as the neutron source throughout the course of this work.

B. Gamma Rays Excited by Inelastic Scattering of 3.8-Mev Neutrons in Nickel, Copper, Zirconium, and Wolfram.

The geometry employed for detection of the gamma rays is shown in Figure 1. All of the measurements obtained to

GEOGRAPHY AND CIRCUITRY OF SCINTILLATION COUNTING EXPERIMENT

Figure 1.



date have been taken by means of single channel pulse-height analysis. A twenty-channel multi-channel discriminator will be available in the future to shorten the time to acquire such data.

As in the case of the previous semi-annual report, the background was taken to be that indicated by a carbon scatterer. The background is assumed to arise from neutrons having been elastically scattered into the sodium iodide and there captured to give rise to capture gamma rays which are in turn counted in the crystal. The carbon run is considered to be a "blank", because the first excited state of C¹² occurs at 4.5 Mev above the ground state so that the neutrons available are not sufficiently energetic to give rise to inelastic scattering. An additional source of background is, of course, the radioactivity of I¹²⁸ ($T = 25$ min.).

A nickel scatterer was constructed of nickel "shot" poured into a thin-walled "doughnut" of tin. When irradiated by 3.8 Mev neutrons, the pulse-height distribution of Figure 2 was obtained. Shown in Figure 2 is the background curve taken with a carbon scatterer present along with the curve for the nickel scatterer. The difference curve is presented in Figure 3 where a photopeak at about 1.36 Mev is clearly present. Although sufficient energy is present for excitation of the 2.52 Mev level in Ni⁶⁰ so that the 1.16 Mev gamma ray might also appear, it is thought that insufficient angular

Figure 2.

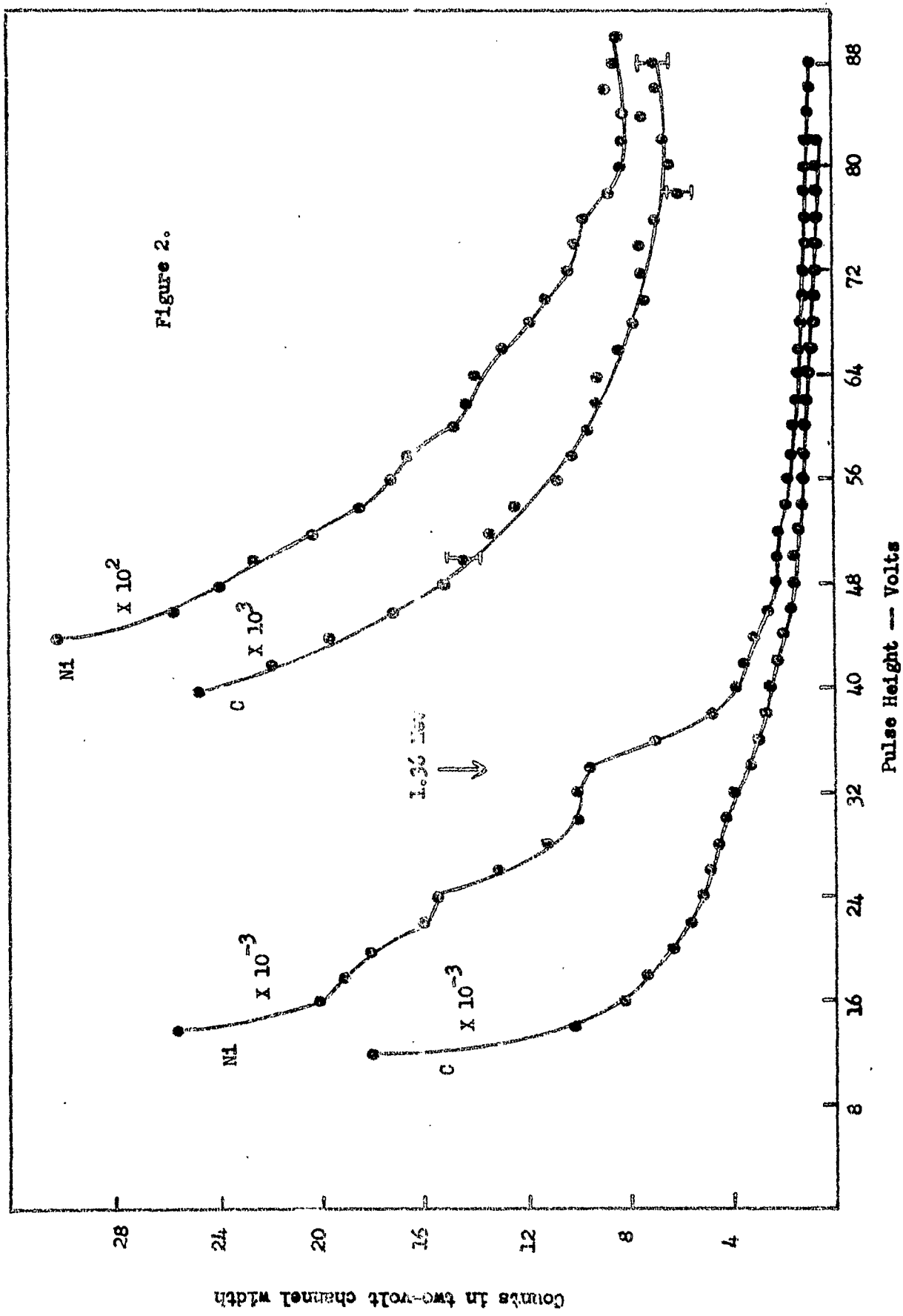
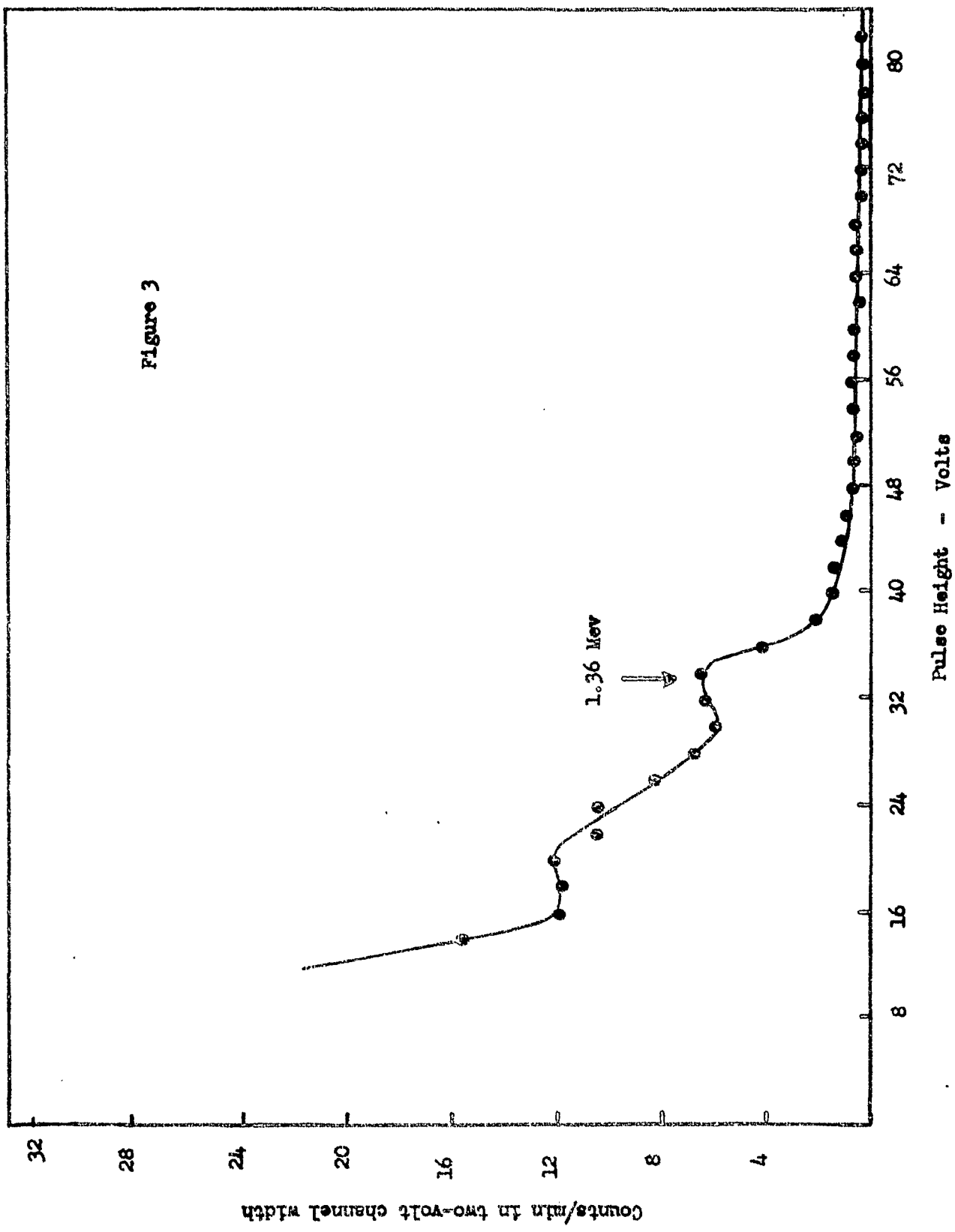


Figure 3



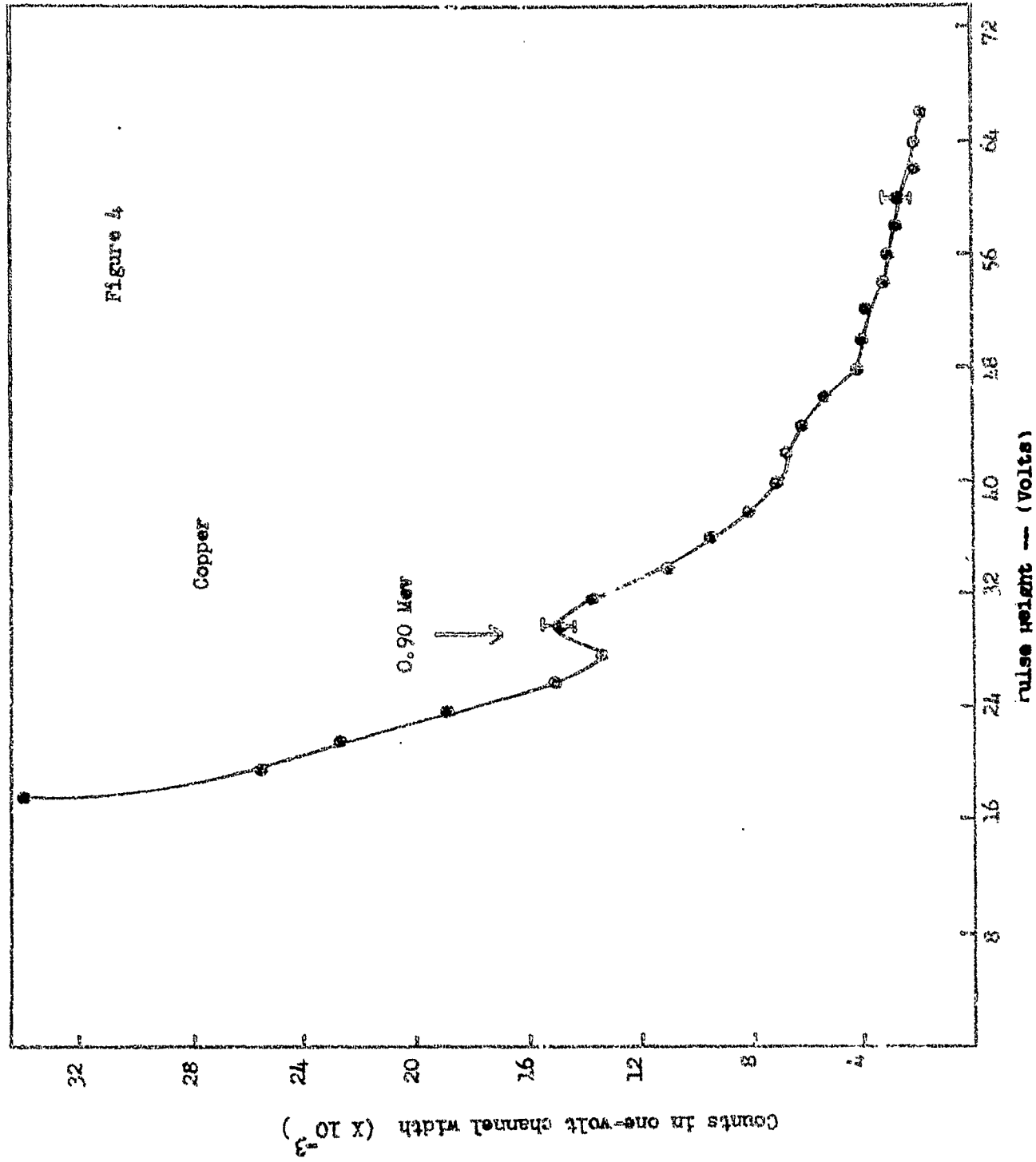
momentum is present in the incident neutron beam to excite the level in any appreciable intensity. The study of the radioactive decay of Co⁶⁰ has shown that the spins of the levels of Ni⁶⁰ follow the pattern of the even-even nuclei, 4 - 2 - 0, so that four units of angular momentum are necessary for excitation of the 2.52 Mev level. The 1.33 Mev gamma ray is of course the second of two gamma rays emitted in cascade in the decay of Co⁶⁰, the first having an energy of 1.16 Mev. From the shape of the difference curve of Figure 3, it is clear that a gamma ray at about 0.9 Mev may also be present.

The pulse-height distribution (background subtracted) resulting from the scattering of 3.8 Mev neutrons by copper is shown in Figure 4. These data are interpreted as giving evidence of the presence of a gamma ray of energy 0.9 Mev, plus unresolved gamma rays of higher energy.

A zirconium scatterer was irradiated by 3.8 Mev neutrons. The resulting pulse-height distribution is shown in Figure 5. The gamma rays present have energies of 0.9, 2.2, and possibly 1.15 Mev. A similar spectrum for tungsten is shown in Figure 6. The resolution is not sufficient to isolate the peaks, but gamma rays appear to be present at about 0.85 and 2.3 Mev.

It is to be noted that the pulse-height distribution curves for Zr was taken with a one-volt channel rather than

Figure 4



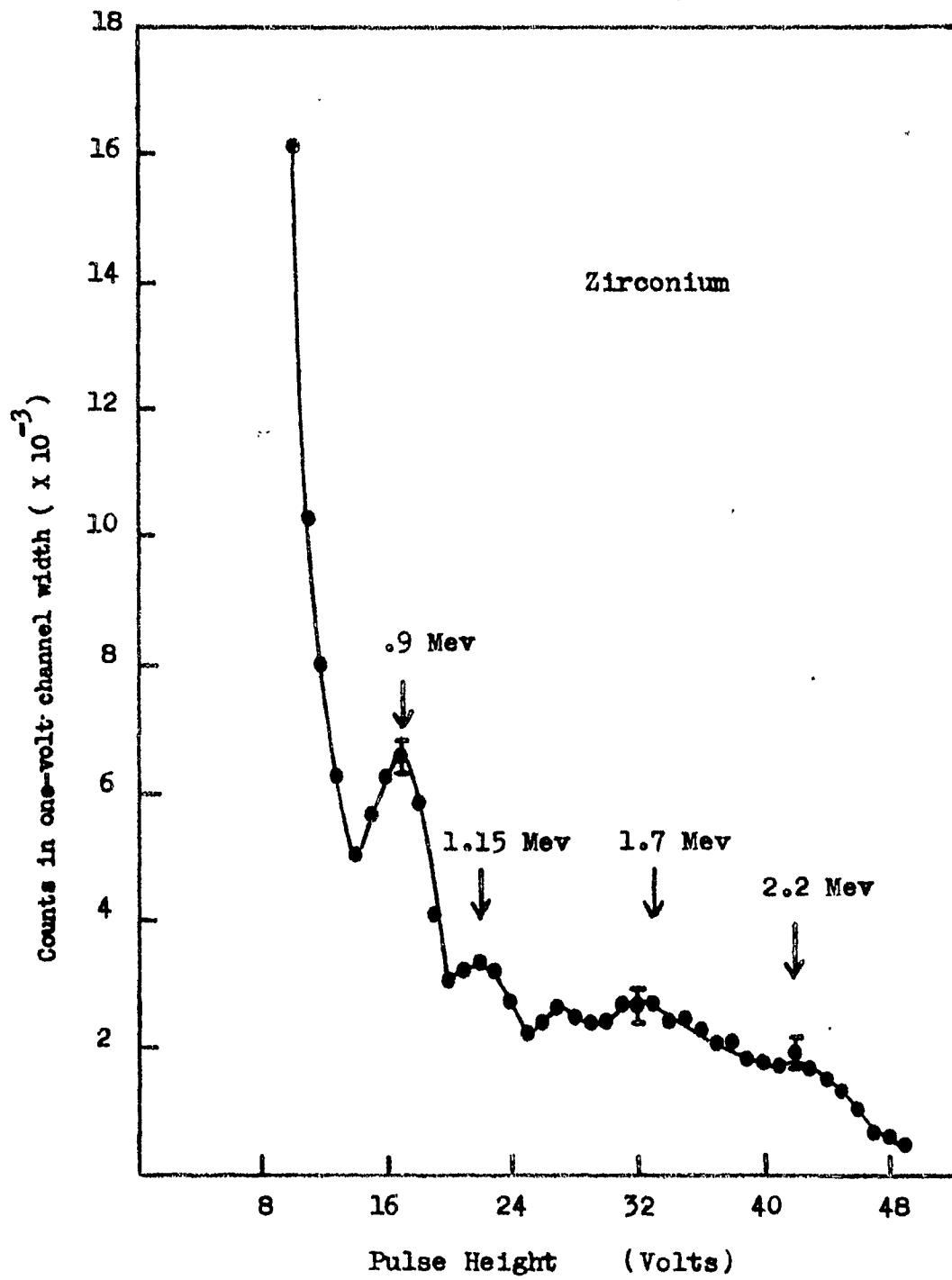
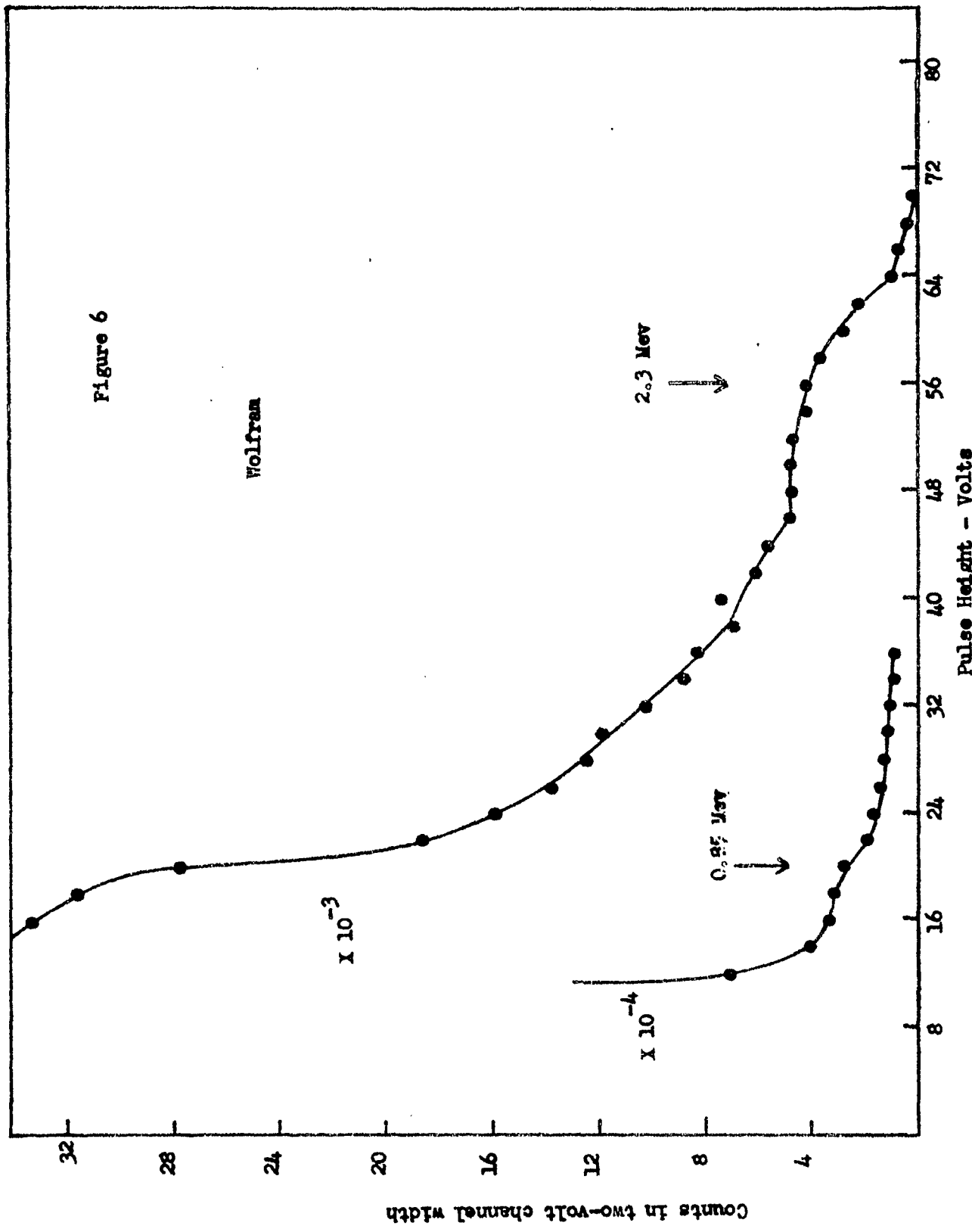


Figure 5

Figure 6



7

with the usual two-volt width employed in the measurements of the previous report. It was found that the use of the one-volt channel resulted in better energy resolution than was previously obtained. Using the one-volt channel, the pulse-height distribution of the gamma rays of Na^{24} was observed as shown in Figure 7. This spectrum shows considerably better resolution than that obtained in the case of the same spectrum obtained with a two-volt channel width and shown in Figure 10 of the previous report. It is naturally to be expected that the one-volt channel give the better resolution; however, the actual experimental observations show that it is enough better to justify the longer time of observation necessitated by the smaller channel widths.

Figure 7

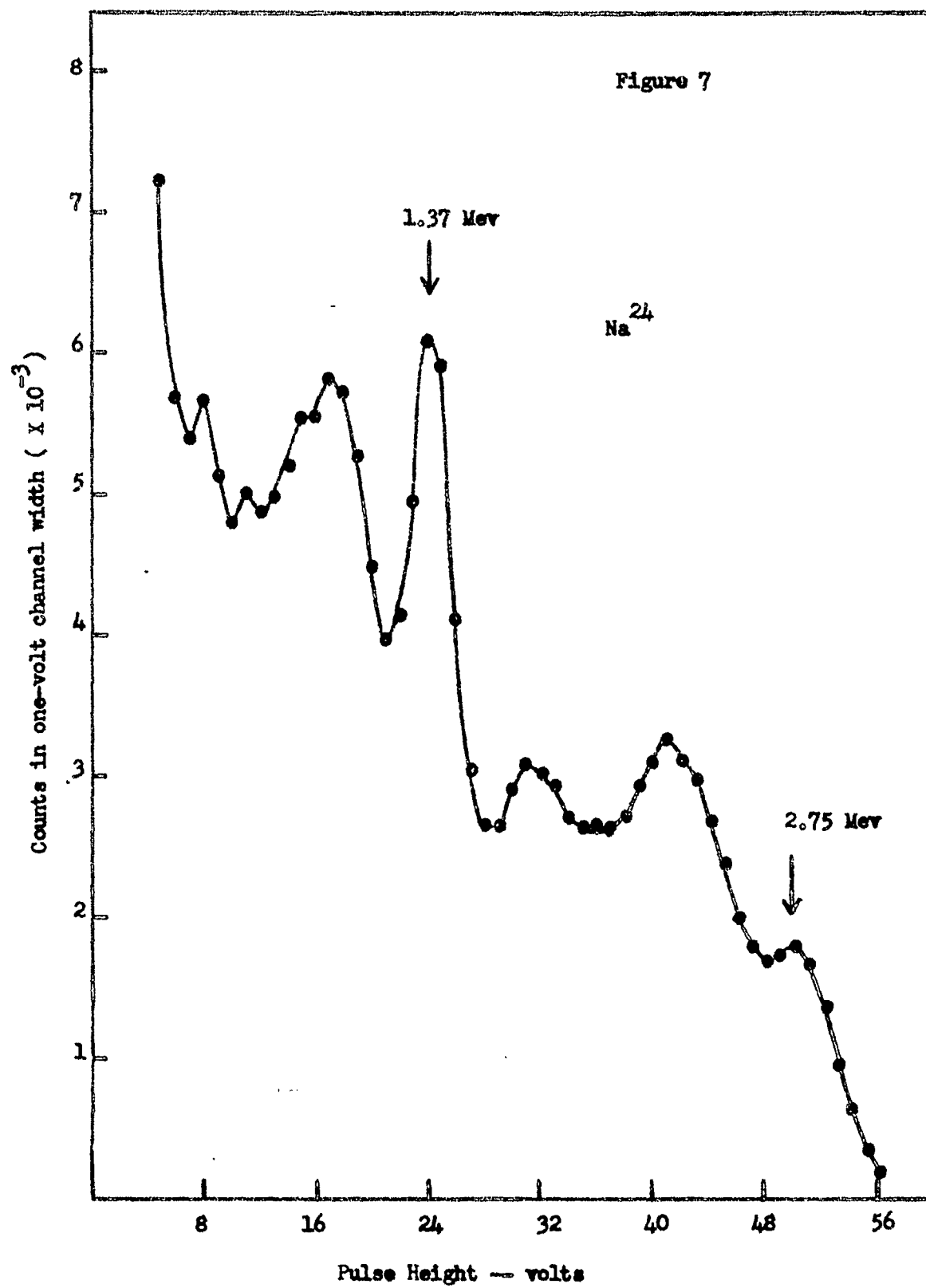


TABLE I

Gamma Rays Excited by 3.8 Mev Neutrons	
Element	Energy of Gamma Ray (Mev)
Nickel	0.9 1.36
Copper	0.9
Zirconium	0.9 1.15 (?) 2.2

7

II. TOTAL CROSS SECTIONS; ANGULAR DISTRIBUTION OF
ELASTIC SCATTERING; INELASTIC CROSS SECTIONS.

Introduction

The measurement of the differential cross sections for the scattering of 3.7 Mev neutrons from cadmium, tin, and bismuth represents an extension of similar measurements¹⁾

1) W. D. Whitehead and S. C. Snowdon, Phys. Rev. 92, 114 (1953)

on aluminum, iron, and lead in order to establish the pattern of variation with atomic weight. In addition, the recent continuum theory of nuclear reactions given by Feshbach, Porter and Weisskopf²⁾ has been used with a

2) Feshbach, Porter and Weisskopf, Phys. Rev. 90, 116 (1953); "Neutron Reactions and the Formation of the Compound Nucleus", U. S. Atomic Energy Commission, NYO 3076, NDA Report 15B-4 (unpublished); "Theory of Average Cross-Sections", M.I.T. Report (unpublished).

plausible extension to calculate the angular distribution of 3.7 Mev neutrons scattered from nuclei of atomic weight 115 and 209. This should be of value in assessing the possibilities of using the continuum theory in this energy range to give detailed information about neutron scattering.

Experimental

In general, the arrangement used in this experiment is exactly the same as that used in our previous experiment¹⁾. Neutrons of about 3.7 Mev were produced by bombarding a deuterium gas chamber with 10 μ a. of deuterons of 0.65 Mev mean energy. A ring geometry was employed in which the angle of scattering was varied both by using different size rings and by an axial movement of each ring.

The previous experiments demonstrated that corrections of considerable magnitude must be made to allow for the higher order scattering in order to obtain the correct differential cross sections from the apparent differential cross sections observed with a ring of finite thickness. They further demonstrated that, within the experimental accuracy, a linear extrapolation of the apparent differential cross section to zero axial thickness of the scatterer most probably gave the correct differential cross section. The present measurements, therefore, were carried out using only two ring thicknesses. However, unlike the previous experiments in which only a few selected angles were chosen to determine the higher order scattering correction, in these experiments each ring thickness was used at all the angles of measurement. The result gives the apparent differential cross section as a function of angle for each of the two ring thicknesses used. The true differential cross

section now can be found at each angle by a linear extrapolation of the apparent differential cross section to zero ring thickness.

Finally, the neutron flux monitor was changed from that previously used, a butane filled proportional counter, to a Lucite-zinc sulphide scintillator detector³⁾ identical

3) W. F. Hornyak, Rev. Sci. Instr. 23, 264 (1952). The authors are indebted to Dr. Hornyak for supplying them with Lucite-zinc sulphide molded buttons.

with that used in detecting the scattered neutrons. In the previous experiments¹⁾ some difficulty was experienced in maintaining a constant $0^\circ/90^\circ$ neutron flux ratio. Changing the monitor-detector improved this situation somewhat.

Data

Figure 1 shows the experimental points of the apparent differential cross section for the scattering of 3.7 Mev neutrons incident on the 3/8 inch and 1 inch thick rings of cadmium. A point by point linear extrapolation to zero ring thickness gives the true differential cross section $\sigma(\theta)$. Figures 2 and 3 present similar information with regard to tin and bismuth. At every angle the apparent differential cross section for the 1-inch rings is larger

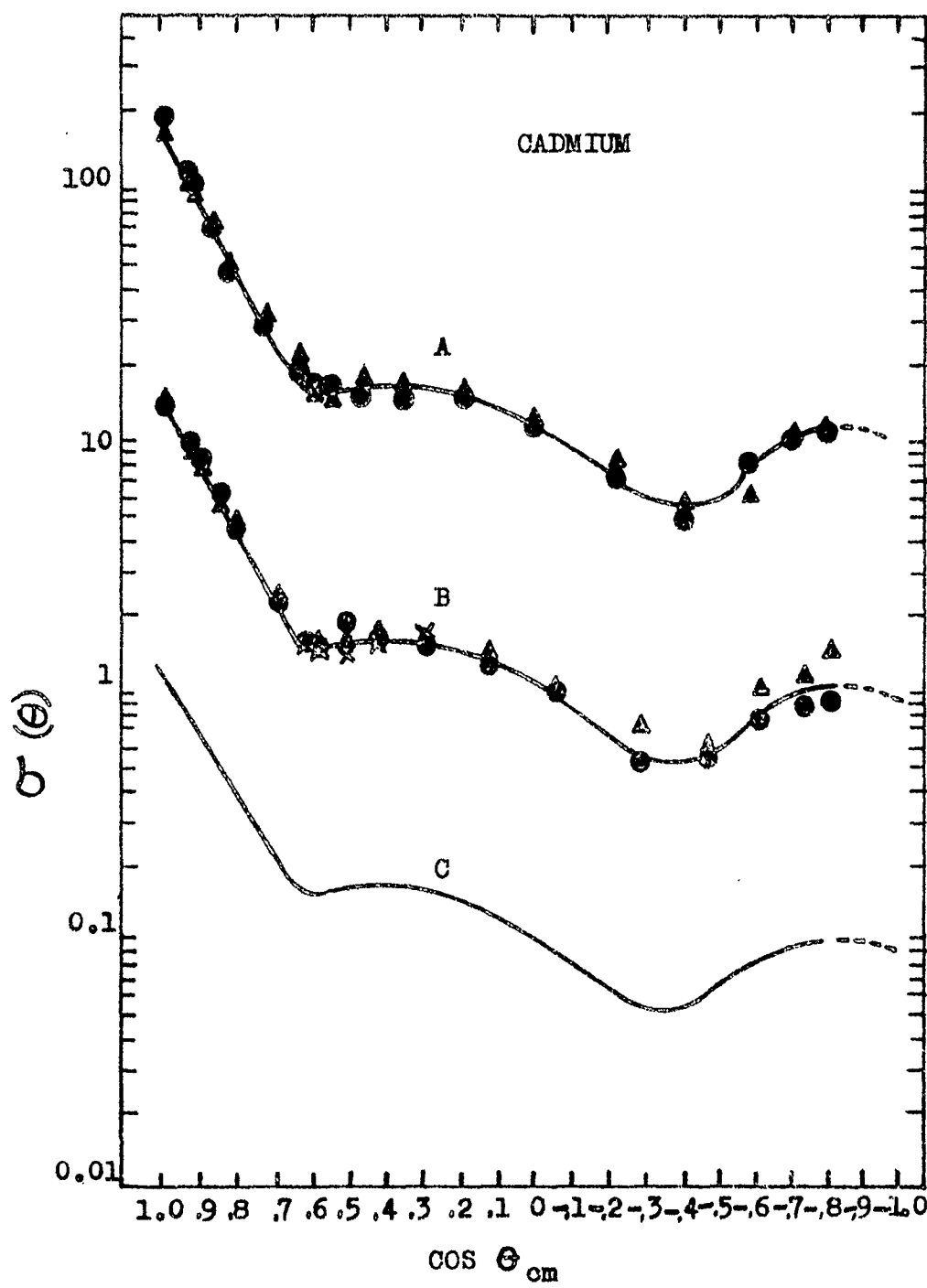


Figure 1

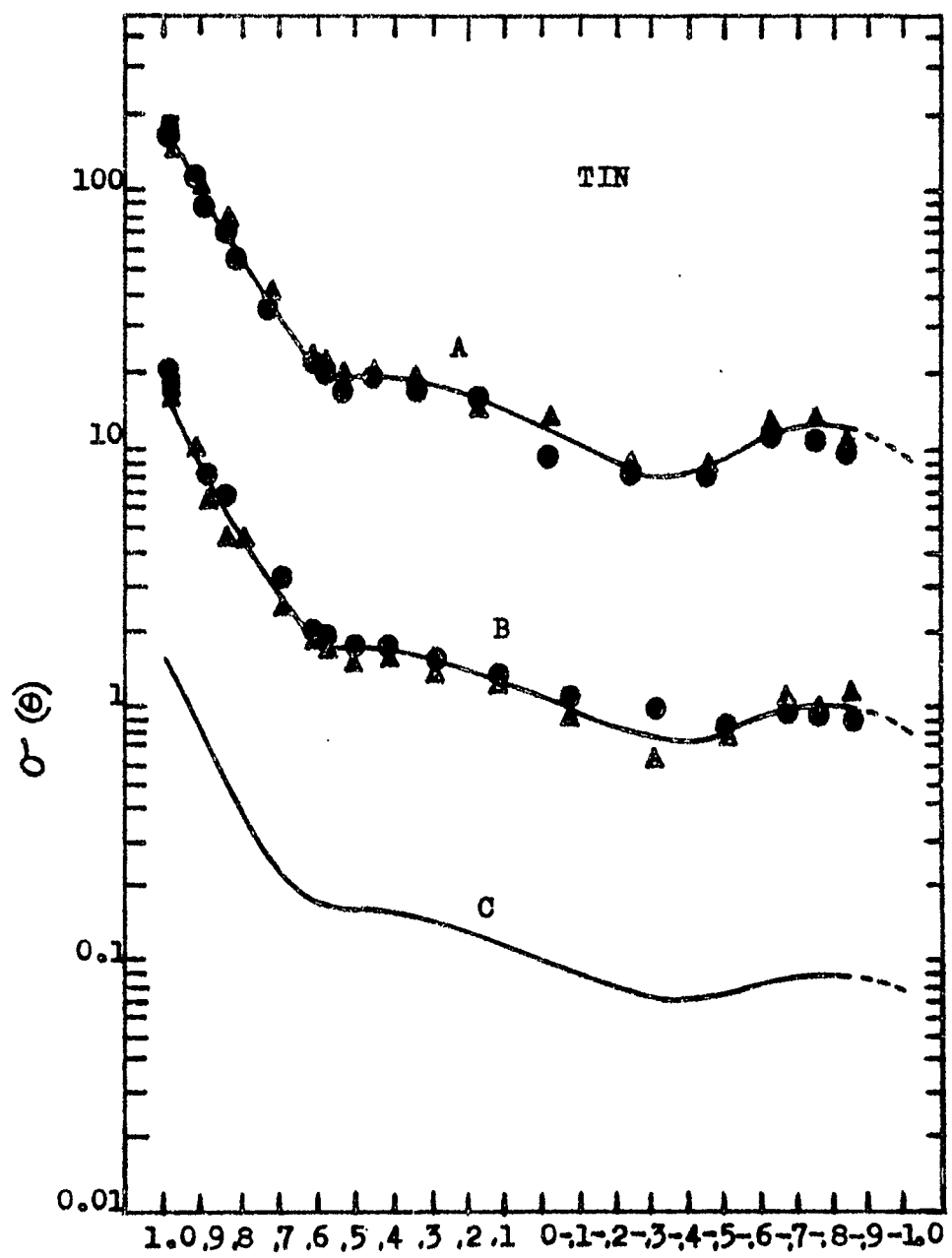


Figure 2

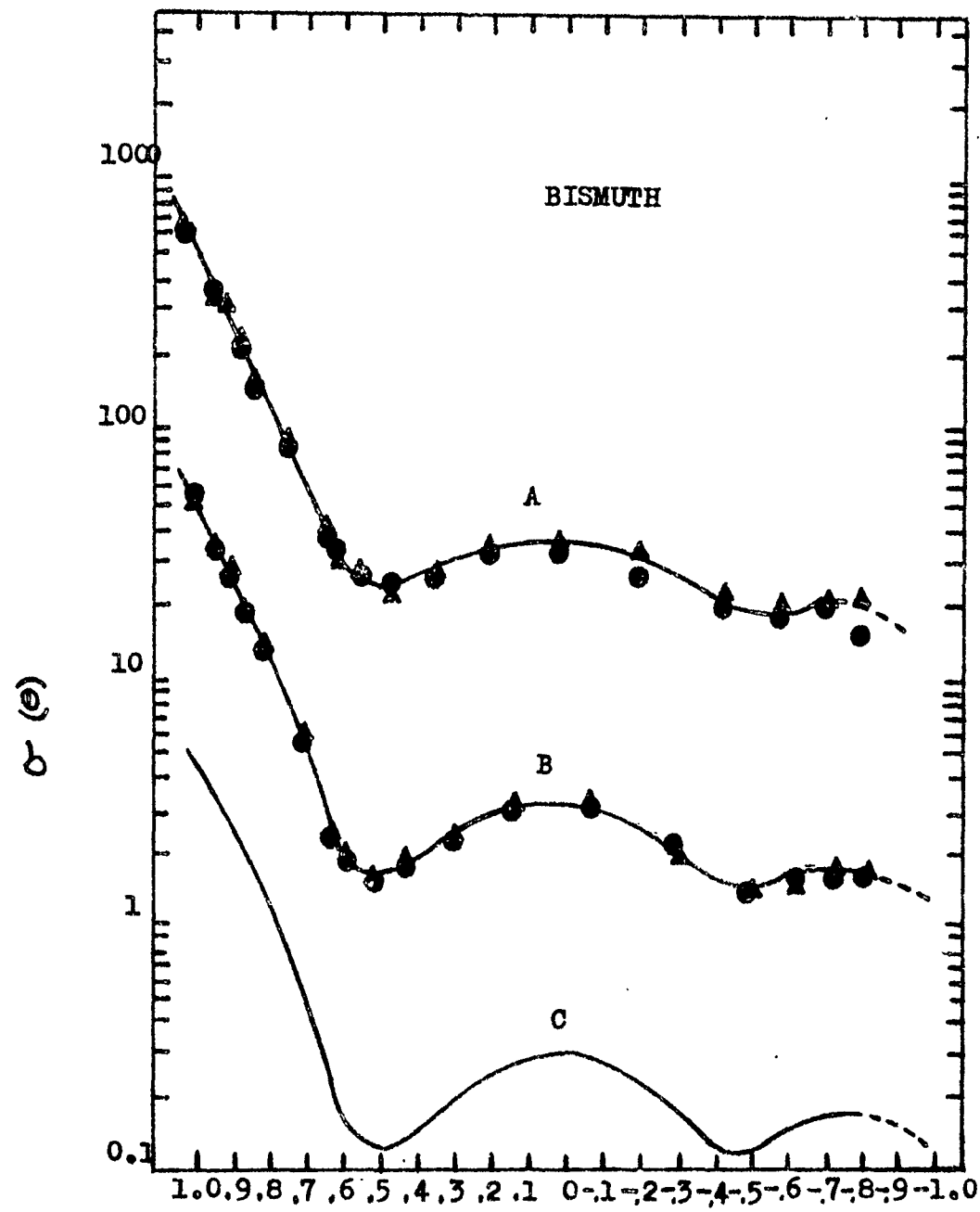


Figure 3

than the apparent differential cross section for the 3/8-inch rings thus demonstrating that at each angle the higher order scattering adds a positive contribution to the apparent differential cross section. The total cross sections corresponding to $\sigma^*(\theta)$ have been calculated and are presented together with the measured total cross sections in Table 1. The measured total cross sections in each case are about 8-10 per cent higher than those previously measured at an energy close to 3.7 Mev⁴⁾.

4) "Neutron Cross Sections", U. S. Office of Technical Services, Department of Commerce, AECU-2040 (unpublished); N. Nereson and S. Darden, Phys. Rev. 89, 775 (1953).

However, since both the differential and total cross sections were measured with the same experimental set-up, at worst all measurements are systematically from 8-10 per cent high which is within our over-all uncertainties of about 15 per cent.

As was discussed previously¹⁾, the integrated cross section corresponding to $\sigma^*(\theta)$ does not accurately measure the total elastic cross section, since the neutron detector does not discriminate adequately against inelastically scattered neutrons. However, to within about 20 per cent, it may be considered to represent this elastic cross section. Subject to this reservation, the difference between the measured total cross section and the integrated

TABLE I.*

Element	σ_{tot} (meas.) in barns			$\int \sigma(\theta) d\ln \theta$ barns	σ_i (inelastic)
	This exp.	Ref. 4	Theory		
Cadmium	4.5	~ 4.0	5.6	2.5	2.0
Tin	4.6	~ 4.2		2.5	2.1
Bismuth	8.3	7.6	7.7	6.9	1.4

Total cross sections. The value of $\int \sigma(\theta) d\ln \theta$ subject to the reservations in the text is the total elastic cross section.

* Included in Table I is a column of values giving estimates of the order of magnitude of the inelastic scattering cross section at 3.7 Mev. Because of errors in the measurement of the total and elastic cross sections, the estimates may be incorrect by as much as a factor of two.

7

cross section corresponding to $\sigma'(\theta)$ may be considered to equal the total inelastic cross section. Table I presents a summary of these calculations.

Theory

Since the neutron energy resolution in this experiment is about 200 Kev, the angular distribution of scattered neutrons may be discussed in terms of a theory that averages the differential cross section over an energy interval of this magnitude. Generally, in our energy range there will be many resonance levels within this 200 Kev energy interval, hence we may average the differential cross section over many resonance levels. Feshbach and Weisskopf⁵⁾ and

5) H. Feshbach and V. F. Weisskopf, Phys. Rev. 76, 1550 (1949); "Final Report of the Fast Neutron Data Project" U. S. Atomic Energy Commission, NYO-636 (unpublished).

Feshbach, Porter and Weisskopf²⁾ have provided two distinct theories that discuss total neutron cross sections averaged in this manner. The total neutron cross-section measurements of Barschall et al⁶⁾. generally show agreement with the theory

6) H. H. Barschall, Phys. Rev. 86, 431 (1952); Miller, Adair, Bockelman, and Darden, Phys. Rev. 88, 83 (1952).

of Feshbach, Porter and Weisskopf²⁾ and are definitely at variance with the theory of Feshbach and Weisskopf⁵⁾.

Therefore, we will compare our measurements with the theory of Feshbach, Porter, and Weisskopf suitably formulated to exhibit the angular distribution of neutrons elastically scattered from nuclei.

The theory first will be formulated, assuming that there are no reaction products (i.e. no inelastic scattering, etc.). In general, the differential cross section for elastic scattering is given by⁷⁾

7) J. M. Blatt and V. F. Weisskopf, *Theoretical Nuclear Physics* (John Wiley and Sons, Inc., New York, 1952) Chapter VIII.

$$\sigma_{sc}(\theta) = \frac{1}{4} \lambda^2 \sum_l \sum_m (2l+1)(2m+1) (1-\eta_l)(1-\eta_m^*) P_l(\cos \theta) P_m(\cos \theta) \quad (1)$$

where λ is the deBroglie wave length of the neutron, divided by 2π , η_l is the phase constant, and $P_l(\cos \theta)$ is the Legendre polynomial. The relation between the phase constant η_l and the corresponding logarithmic derivative f_l if given by⁷⁾

$$\eta_l = \exp(2i f_l) \cdot \left[(f_l - \Delta_l + i s_l) / (f_l - \Delta_l - i s_l) \right] \quad (2)$$

where γ_ℓ is the phase determining the potential scattering, and $\Delta_\ell + i s_\ell$ is the logarithmic derivative of the outgoing wave in the entrance channel.

We now average Eq. (1) over an energy interval that includes many resonance levels

$$\sigma_{SC}(\theta) = \frac{1}{4} \lambda^2 \sum_l \sum_m (2l+1)(2m+1) \left[(1 - \bar{\eta}_\ell) (1 - \bar{\eta}_m^*) + (\bar{\eta}_\ell \bar{\eta}_m^* - \bar{\eta}_\ell^* \bar{\eta}_m) \right] P_\ell(\cos \theta) P_m(\cos \theta) \quad (3)$$

where all quantities such as λ , γ_ℓ , s_ℓ , and Δ_ℓ that only vary slowly with the energy are treated as constants. The distribution obtained from the term $(1 - \bar{\eta}_\ell) (1 - \bar{\eta}_m^*)$ is called the "shape elastic" scattering and the distribution obtained from the term $(\bar{\eta}_\ell \bar{\eta}_m^* - \bar{\eta}_\ell^* \bar{\eta}_m)$ is called the "compound elastic" scattering².

In order to calculate $\bar{\eta}_\ell$, first it is necessary to choose a model that will provide a logarithmic derivative which includes a description of resonances. Feshbach, Porter and Weisskopf introduce a simplified version of a nuclear reaction. The zero order approximate problem is described by a Hamiltonian

$$H^{(0)} = H_T + H_n \quad (4)$$

where H_T is the Hamiltonian describing the complicated internal motions of the target nucleus and H_n describes the relative motion of the neutron and the target and is given by

$$H_n = \frac{\hbar^2}{2m} \nabla^2 + V(r), \quad (5)$$

where m is the reduced mass, ∇^2 is the Laplacian in the relative coordinate of the neutron and the target system. $V(r)$ is given by

$$V(r) = -V_0 \text{ for } r < R; 0 \text{ for } r > R, \quad (6)$$

where R is the nuclear radius.

The formation of the compound nucleus is described in the next approximation by adding an interaction operator H' to give for the total Hamiltonian

$$H = H_T + H_n + H' \quad (7)$$

For a convenient choice of the matrix elements of H' in the basis determined by the eigenfunctions of H_T , the value of the logarithmic derivative may be found. It is shown then that this rather complicated expression for the logarithmic derivative may be approximated by

$$f_\ell = w_{1\ell} + w_{2\ell} \cot z_\ell(\epsilon) \quad (8)$$

where w_1 and w_2 are slowly varying functions of the energy of the neutron ϵ . The phase $z_\ell(\epsilon)$ is taken as proportional to the energy. If this expression for the logarithmic derivative is inserted into Eq. (2) and averaged over many resonances the result is

$$\bar{\eta}_\ell = \exp(2i\zeta_\ell) \cdot \left[(w_{1\ell} - i w_{2\ell} - \Delta_\ell + is_\ell) \right] / \left[(w_{1\ell} - i w_{2\ell} - \Delta_\ell - is_\ell) \right] \quad (9)$$

Thus, the averaging results in replacing the $\cot z_\ell$ in Eq. (8) by $-i$. The expressions obtained for $w_{1\ell}$ and $w_{2\ell}$ in the perturbation calculation are such that they may be approximated by the real and imaginary parts of the logarithmic derivative of the following non-Hermitean problem in the relative coordinates of the neutron and the target

$$H = -\frac{\hbar^2}{2m} \nabla^2 + V(r)$$

where

$$V(r) = -V_0(1 + i\zeta) \text{ for } r < R; 0 \text{ for } r > R \quad (10)$$

Thus, all quantities in Eq. (3) are provided for except $\overline{\eta_\ell \eta_m^*}$. To obtain this we assume in Eq. (8) that

$z(\epsilon)$ is a linear function of the energy

$$z_\ell = \pi\epsilon/d_\ell + \beta_\ell \quad (11)$$

where d_ℓ is the average level separation. The product $\eta_\ell \eta_m^*$ is then averaged with respect to ϵ as in the case of η_ℓ . In particular, the result will depend on the unknown parameters β_ℓ . Since we are only interested in statistical results, the average of $\eta_\ell \eta_m^*$ with respect to ϵ is again averaged with respect to β_ℓ . The result is then

$$\overline{\eta_\ell \eta_m^*} = \bar{\eta}_\ell \bar{\eta}_m^* \text{ for } \ell \neq m; 1 \text{ for } \ell = m \quad (12)$$

Thus, the average phase constant in Eq. (9) completely defines an angular distribution of the elastic scattering averaged over many resonances. The non-Hermitean problem defined by Eq. (10), which is used to provide an approximate expression for the average phase, may be solved by a method due to Lax and Feshbach⁸). We have used for the

8) M. Lax and H. Feshbach, Journ. Acoust. Soc. Amer., 20, 108 (1948); Morse, Lowan, Feshbach and Lax, "Scattering and Radiation from Circular Cylinders and Spheres" (Reprinted by U. S. Navy Department Office of Research and Inventions, Washington, D.C., 1946).

potential within the nucleus

$$V = -19(1 + 0.05 A) \text{ Mev} \quad (13)$$

and for the nuclear radius

$$R = 1.45 \times 10^{-13} A^{1/3} \text{ cm}. \quad (14)$$

These values give good agreement with the total cross-section measurements of Barschall^{2, 6)}.

In the preceding theory, it was assumed that no reaction products were present in the decay of the compound nucleus. This restriction may be removed by realizing that the effect of these reaction products upon the entrance channel can be accounted for approximately by introducing an imaginary part to the energy. Thus, Eq. (11) is changed to

$$z_\ell = \frac{\pi}{d_\ell} \left(\epsilon + i \Gamma_r^{(\ell)} / 2 \right) + \beta_\ell \quad (15)$$

where $\Gamma_r^{(\ell)}$ is the reaction width^{2, 9)}. When this is

⁹⁾ Feshbach, Peaslee and Weisskopf, Phys. Rev. 71, 145 (1947).

done it will be found that Eq. (9) for the average phase $\bar{\eta}_\ell$ is unchanged and that Eq. (12) for the average phase product $\bar{\eta}_\ell \bar{\eta}_m^*$ is unchanged for $\ell \neq m$ but that for $\ell = m$

$$\bar{\eta}_\ell \bar{\eta}_m^* = 1 - (\exp 2\pi \Gamma_r^{(\ell)} / d_\ell - 1)(1 - \bar{\eta}_\ell \bar{\eta}_\ell^*) / [\exp 2\pi \Gamma_r^{(\ell)} / d_\ell - \bar{\eta}_\ell \bar{\eta}_\ell^*] \quad (16)$$

Hence, the preceding formulation may be used throughout except for this one change. Table 2 and Figures 4-6 present the chief numerical results of the above theory.

Discussion

A comparison in Figures 4-6 of the experimental differential cross section for the elastic scattering of 3.7 Mev neutrons from cadmium, tin, and bismuth with the theoretical predictions of the continuum model shows that the main features of the experimental curves are reproduced by the theory. In general, the theoretical results give a better fit with bismuth than with cadmium or tin. If one were to use Eq. (16) in the determination of the "compound elastic" scattering, there is no choice of the ratio of reaction width to level separation $\Gamma_r^{(\ell)} / d_\ell$ that would make the fit much better. The addition of "compound elastic" scattering, however, does adjust the "shape elastic" scattering to a distribution that more nearly

TABLE 2.

$R(10^{-13} \text{ cm})$	σ_{se} (barns)	$\overline{\sigma}_c$ (barns)	$\overline{\sigma}_{tot}$ (barns)
7.1 (Cd, Sn)	4.0	1.6	5.6
8.6 (Bi)	6.1	1.6	7.7

σ_{se} is the integrated "shape elastic" cross section. $\overline{\sigma}_c$ is the average cross section for the formation of the compound nucleus. $\overline{\sigma}_{tot}$ is the total neutron cross section. The "compound elastic" cross section plus the average reaction cross section add up to $\overline{\sigma}_c$.

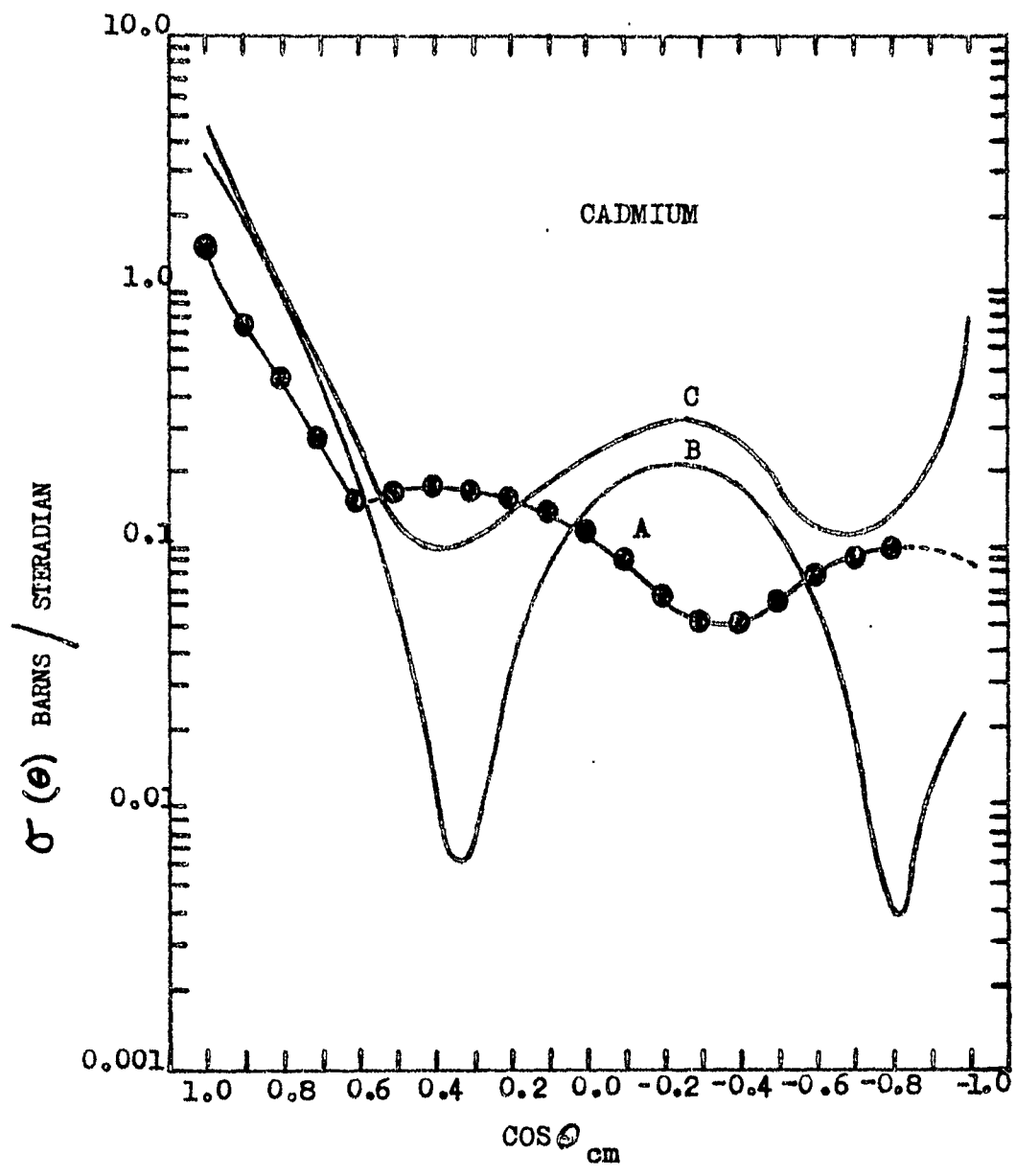


Figure 4.

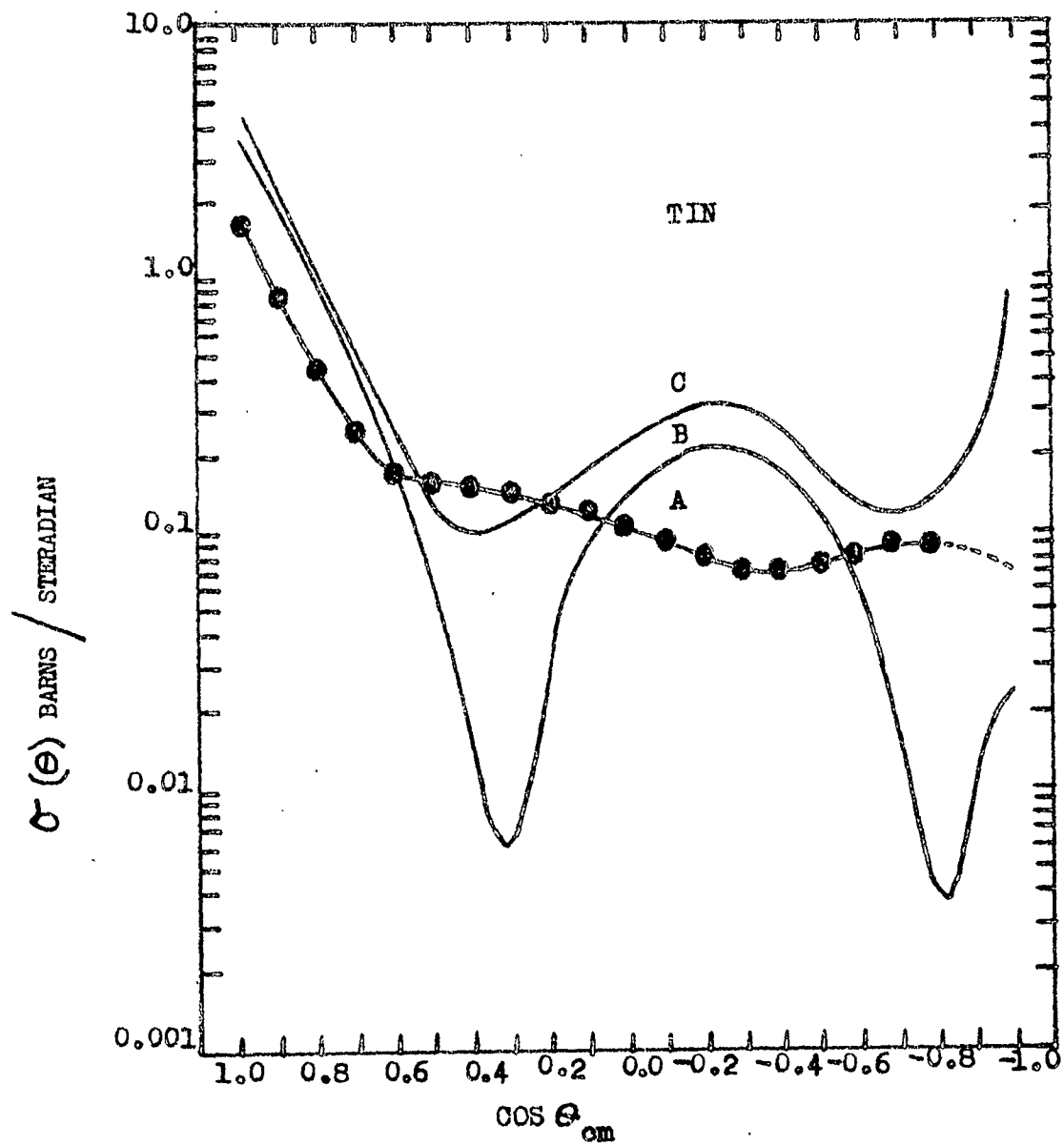


Figure 5.

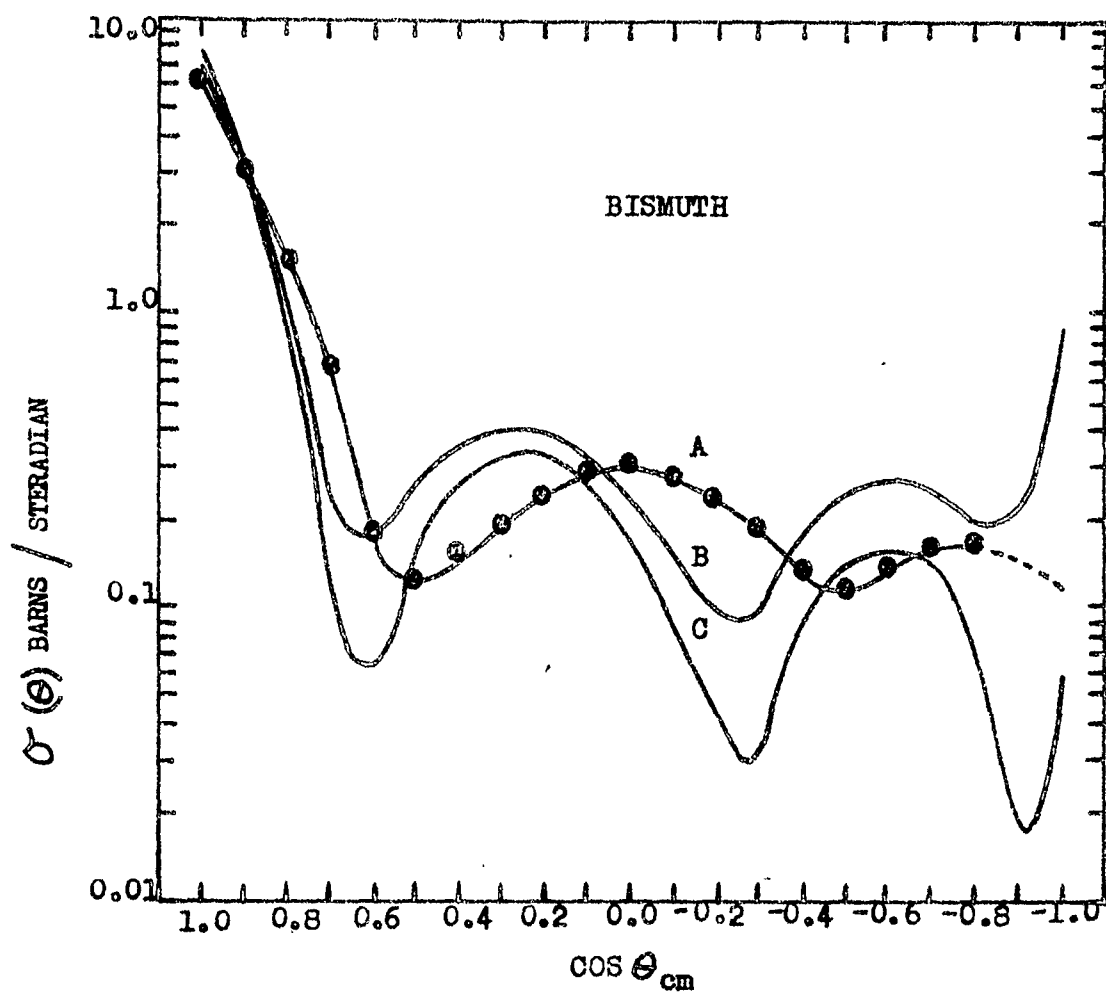


Figure 6

resembles the experimental curve than does the "shape elastic" scattering alone. In particular, this "compound elastic" scattering shifts the position of the first minima in the "shape elastic" scattering. Since different nuclei have different amounts of "compound elastic" scattering, this may account for the lack of a uniform shift in the position of the first minima in the experimental elastic-scattering distributions as one proceeds from iron to bismuth.

Since the largest discrepancy between theory and experiment occurs in the differential cross section for forward-scattering, $\sigma_{sc}(0)$, it is of interest to consider possible adjustments of $\sigma_{sc}(0)$ in the theory. The minimum theoretical value of $\sigma_{sc}(0)$ is given by a theory that does not include "compound elastic" scattering and has the maximum possible cross section for the formation of the compound nucleus. These conditions are met in the first version of the continuum theory⁵⁾. The values of $\sigma_{sc}(0)$ from this theory agree with the experimental value of $\sigma_{sc}(0)$ in the case of bismuth but are too high in the case of cadmium and tin. In the case of bismuth, however, the subsequent form of $\sigma_{sc}(\theta)$ does not offer any possibility of giving a detailed fit. Therefore, it is not possible to obtain a useful value of $\sigma_{sc}(0)$ that agrees with experiment by adjusting only the value of ζ in Eq. (13) and the value of $\Gamma_r^{(l)} / d_l$ in Eq. (16). It can be argued

7

that the double average used to obtain $\overline{\eta_l \eta_m^*}$ in Eq. (12), strictly speaking, is not a necessary feature of the continuum theory and that one should insert some function of ℓ for the parameter β_ℓ in Eq. (11). To get some idea of the restriction introduced by this average over β_ℓ , the value of $\eta_l \eta_m^*$ was averaged with respect to ϵ with the value of β_ℓ set equal to zero. For bismuth the difference between this method and the double average method was quite small. For cadmium and tin the difference was somewhat larger but still not large enough to alter appreciably the results of the double average method. Hence, it is not likely that significantly better fits between theory and experiment would be obtained if β_ℓ were known as a function of ℓ .

Since the theoretical value of $\sigma_{sc}^{(0)}$ can be made to agree with experiment by adjusting the nuclear radius, it is of interest to estimate the magnitude of the change necessary to bring about this agreement. The nuclear radius used for bismuth ($A = 209$ in Eq. (14)) would have to be lowered by about 6 per cent since $\sigma_{sc}^{(0)}$ varies approximately as the fourth power of the radius. This also would move the first theoretical minima closer to the first experimental minima. Since this change in radius would lower the total cross section by approximately 15 per cent and since the total cross section is in fair agreement with

experiment, it would be necessary to raise the imaginary part of the potential in Eq. (13) by about 15 per cent in order to maintain agreement of the theoretical and experimental total cross section. Furthermore, a lowering of the nuclear radius by about 6 per cent would be in agreement with the measurements of Coon, Graves, and Barschall¹⁰⁾, in which they find

10) J. H. Coon, E. R. Graves, and H. H. Barschall,
Phys. Rev. 88, 562 (1952).

for 14 Mev neutrons and for elements above barium that the nuclear radius as measured by $(\sigma_{tot}/2\pi)^{1/2}$ falls below the value predicted by $R = 1.5 \times 10^{-13} A^{1/3}$ cm.

In order to adjust the theory to the experimental value of $\sigma_{sc}(0)$ for cadmium and tin it would be necessary to lower the nuclear radius chosen ($A = 115$ in Eq. (14)) by about 30 per cent. Corresponding to this, it would be necessary to increase the parameter ζ by a large amount to give a sufficiently large total cross section if, indeed, a large change in ζ is capable of adjusting the total cross section by a correspondingly large amount. This large adjustment of the nuclear radius is not very palatable in view of the general experimental agreement of the nuclear radius with the formula in Eq. (14) for 14 Mev neutrons and for values

of A near $115^{10)}$. It is conceivable that the theory as it stands would give better agreement if it were applied to an ellipsoidal-shaped target nucleus. However, since only 20-25 per cent of the cadmium and tin isotopes have odd neutron numbers and since nuclear eccentricities in the region of $A = 115$ are only about 6 per cent¹¹⁾, it is not likely that the use of an

11) J. M. Blatt and V. F. Weisskopf, "Theoretical Nuclear Physics" (John Wiley and Sons, Inc., New York, 1952) pp. 29, 776.

ellipsoidal-target nucleus can produce the desired change. Hence, we are reduced to the necessity of a modification of the theory as the only means by which a sufficiently large adjustment can be accomplished. Within the general framework of the theory, it might be possible to choose the matrix elements of H^1 in Eq. (7) to be a function of the relative coordinate, r , or to let the potential in Eq. (6) be a function of the spins of the neutron and the target nucleus¹²⁾. In any case, however, it would be necessary

12) N. C. Francis and K. M. Watson, Phys. Rev. 92, 291 (1953).

that these changes introduce little effect on the present results in the neighborhood of $A = 209$.

7

In summary then, it may be said that the continuum theory may be brought into rather detailed agreement with the measured angular distribution of 3.7 Mev neutrons scattered from bismuth. The theory in the case of cadmium and tin exhibits only the general features of the experimental results and possibly demonstrates a need for a revision of the theory.

Captions for Figures

Figure 1 - Angular distribution of 3.7 Mev neutrons scattered from cadmium. (A) apparent differential cross section using 1" axial thickness ring scatterers. (B) apparent differential cross sections using 3/8" axial thickness ring scatterers. (C) true differential cross sections for elastic scattering obtained by a point-by-point linear extrapolation of curves (A) and (B) to zero thickness scatterer. Ordinates are for curve (C) and are in units of barns/steradian. Curve (B) ordinate should be reduced by a factor of 10. Curve (A) ordinate should be reduced by a factor of 100.

Figure 2 - Angular distribution of 3.7 Mev neutrons scattered from tin. (A) apparent differential cross section using 1" axial thickness ring scatterers. (B) apparent differential cross section using 3/8" axial thickness ring scatterers. (C) true differential cross section for elastic scattering obtained by a point-by-point linear extrapolation of curves (A) and (B) to zero thickness scatterer. Remarks concerning ordinates are the same as in Figure 1.

7

Captions for Figures (Continued)

Figure 3 - Angular distribution of 3.7 Mev neutrons scattered from bismuth. (A) apparent differential cross section using 1" axial thickness ring scatterers. (B) apparent differential cross section using 3/8" axial thickness ring scatterers. (C) true differential cross section for elastic scattering obtained by a point-to-point linear extrapolation of curves. (A) and (B) to zero thickness scatterer. Remarks concerning the ordinates are the same as in Figure 1.

Figure 4 - Comparison of the experimental differential cross section for the elastic scattering of 3.7 Mev neutrons from cadmium with the predictions of the continuum model for a nuclear radius of 7.1×10^{-13} cm and a complex potential constant of $-19(1 + 0.05 i)$ Mev. (A) experimental results from Figure 1(C). (B) "Shape elastic" differential cross section. (C) "Compound elastic" plus "shape elastic" differential cross section using Eq. (12) to determine the "Compound elastic" scattering. Solid triangle is $\sigma_{sc}^{(0)}$ from first version of the continuum theory.

Figure 5 - Comparison of the experimental differential cross section for the elastic scattering of 3.7 Mev neutrons from tin with the predictions of the continuum model

Captions for Figures (Continued)

for a nuclear radius of 7.1×10^{-13} cm and a complex potential constant of $-19(1 + 0.05 i)$ Mev. (A) experimental results from Figure 2(C). (B) "shape elastic" differential cross section. (C) "compound elastic" plus "shape elastic" differential cross section using Eq. (12) to determine the "compound elastic" scattering. Solid triangle is $\sigma_{sc}(0)$ from first version of the continuum theory.

Figure 6 - Comparison of the experimental differential cross section for the elastic scattering of 3.7 Mev neutrons from bismuth with the predictions of the continuum model for a nuclear radius of 8.6×10^{-13} cm and a complex potential constant of $-19(1 + 0.05 i)$ Mev. (A) experimental results from Figure 3(C). (C) "shape elastic" differential cross section. (B) "compound elastic" plus "shape elastic" differential cross section using Eq. (12) to determine the "compound elastic" scattering. Solid triangle is $\sigma_{sc}(0)$ from first version of the continuum theory.

III. LOW VOLTAGE ACCELERATOR

In a previous report there is described a bench test ion source assembly used to study operating characteristics of the Bartol radiofrequency ion source. As part of the projected program concerning scattering studies on neutrons it was decided to convert this test bench into a positive ion accelerator which would operate at voltages up to 100 Kv. The chief advantage of this type of accelerator for neutron studies is the provision of a beam current several times greater than those obtained from the Van de Graaff generator and having sufficient energy to yield a reasonable flux of neutrons from the exothermic reactions, $H^2(d,n)He^3$ and $H^3(d,n)He^4$.

It was decided to incorporate an ion source developed at Oak Ridge which differs from the source used in the Van de Graaff generators in that it provides considerably larger beam currents. An ion source of this type was obtained from Oak Ridge and installed in the accelerator last fall.

It became apparent at that time that the completion of the large generator and continual use of the smaller generator would prohibit satisfactory operation of a third accelerator in the same room, and accordingly plans were

made to renovate a garage on the Bartol property for purposes of housing the low-voltage accelerator. In April the building was completed and the accelerator moved to the second floor. During the spring and summer several structural changes were made to provide more convenient and stable operation. In particular, provision was made for extension of the tube through the floor into the middle of the room below in order to reduce as far as practicable the problems associated with scattering of the neutrons from floor and walls.

After several initial difficulties with the vacuum system and adjustments on the ion source a beam of 120 μ a has been focused on a target 1 1/2" in diameter at a distance of 10 feet from the source. A liquid air-cooled system was installed in order to freeze D_2O onto the metal target for producing neutrons from the $H^2(d,n)He^3$ reaction.

7

IV. INELASTIC SCATTERING OF NEUTRONS BY Ba¹³⁷ and Hg¹⁹⁹ *

C. P. Swann and F. R. Metzger

Bartol Research Foundation of The Franklin Institute, Swarthmore, Pa.

Abstract

The production by inelastic scattering of neutrons of the 527 kev isomeric level of Hg¹⁹⁹ and of the 661 kev isomeric level of Ba¹³⁷ have been studied. Neutrons were produced by bombarding a 50 kev lithium target with protons accelerated in the large Bartol Van de Graaff. The cross section for the production of the 13/2+ level of Hg¹⁹⁹ increases sharply at 620 ± 10 kev mean neutron energy indicating a level at about 90 kev above the metastable state. Below 620 kev the observed activity decreases with increasing neutron energy and is attributed mainly to fast neutron capture by Hg¹⁹⁸. At 620 kev the cross section corresponds to about one mb. Several other breaks indicate higher excited states in Hg¹⁹⁹. The 11/2- level of Ba¹³⁷ has been excited with mean neutron energies as low as 670 ± 10 kev indicating direct formation of the metastable state. The experimental cross section at 150 kev above the threshold is about 5 mb which is an order of magnitude smaller than the theoretical estimate based on
1) the compound nucleus model.

* Supported in part by the U. S. Atomic Energy Commission and in part by the joint program of the U.S. Office of Naval Research and the U. S. Atomic Energy Commission.

1) W. Hauser and H. Feshbach, Phys. Rev. 87, 366 (1952).

V. RECENT PUBLICATIONS

Recently published works carried out under this Contract are:

"Nuclear Emulsion Method for Energy Measurement of Inelastically Scattered Neutrons", by S. C. Snowdon, M. A. Rothman, D. W. Kent, Jr., and W. D. Whitehead, Rev. of Scientific Instr., Vol. 24, No. 9, 876-877, September, 1953.

"Angular Distribution of Neutrons Scattered from Aluminum, Iron, and Lead", by W. D. Whitehead and S. C. Snowdon, Phys. Rev., Vol. 92, No. 1, 114-119, October 1, 1953.

Nuclear Emulsion Method for Energy Measurement of Inelastically Scattered Neutrons*

S. C. SNOWDON, M. A. ROTIMAN, D. W. KENT, JR.,
AND W. D. WHITEHEAD
*Bartol Research Foundation of The Franklin Institute,
Swarthmore, Pennsylvania*
(Received April 1, 1953)

NUCLEAR emulsions have been used for some time in what may be called a point source of neutron geometry (point geometry) to record the energy spectrum of neutrons produced in nuclear reactions. The same method applied to the observation of inelastically-scattered neutrons has two defects: (a) the source of bombarding particles is relatively weak because these particles first must be produced by a nuclear reaction in order to get monoenergetic neutrons; (b) the bombarding neutrons as well as the scattered neutrons give proton recoils in the emulsion. The purpose of this letter is to present a method of overcoming these defects. Since the low intensity of flux incident on the scatterer cannot be increased appreciably, one can only hope to arrange the scatterer geometry so that many scattering points give similar contributions to the proton recoil spectrum. In order to prevent the direct neutron flux from producing a proton recoil spectrum comparable with that from the scatterer, it is necessary that the plane of the emulsion be placed at right angles to the incident flux. Both of these conditions are met if the scattering material is placed in an axially symmetric ring (ring geometry), and the photographic emulsion is located on the axis with its plane in the central plane of the ring (Fig. 1).

In order to utilize the ring geometry, the customary acceptance criteria¹ must be changed to the following single criterion: all proton recoil tracks are acceptable if their angle of dip with respect to the plane of the emulsion is less than θ_0 . In our case $\theta_0 = 12^\circ$. The feasibility of the ring geometry will have been ascertained if a calculation is made of the recoil proton spectrum from the following sources of scattered neutrons: (1) the ring (signal); (2) all elements in the emulsion (noise); and (3) the boundaries of the room (noise).

It should be noted that the noise of type (2) may be reduced by interposing some scattering material on the axis between the neutron source and the emulsion. Also, there will be a proton spectrum in the emulsion because of the $\text{N}^{14}(n, p)$ reaction ($Q = 0.627 \text{ Mev}$).² This spectrum may easily be distinguished from the scattering spectrum, first because it will have a line spectrum, and secondly, because of the positive Q value, the peak will occur at an energy appreciably higher than that of the scattered neutron spectra.

In order to investigate points (1) and (2), it will be assumed that

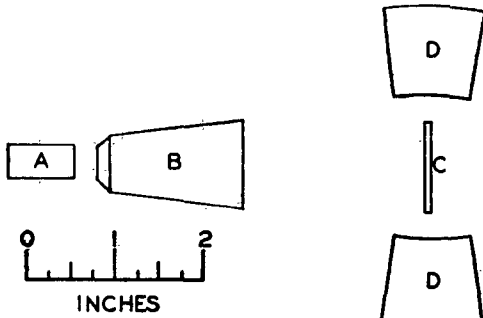


FIG. 1. Ring geometry for scatterer: (A) deuterium gas at one-half atmosphere pressure to give neutrons of 4 Mev from the D-D reaction; (B) copper shield that attenuates the direct neutron flux on the emulsion by 1/e; (C) 330-micron NTA pellicle of about one inch diameter; (D) ring scatterer 6 inch i.d., 8 inch o.d., 12° half-angle from center of emulsion.

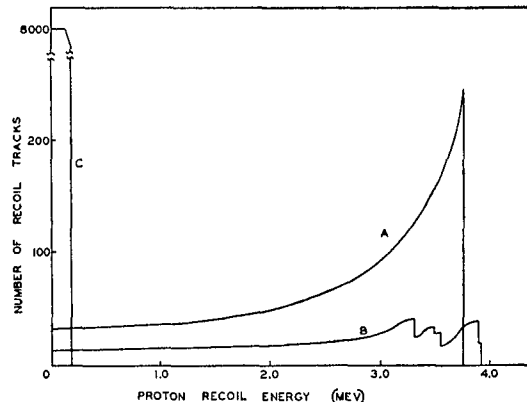


FIG. 2. Proton recoil spectra: (A) Signal spectrum of neutrons elastically scattered from iron for a 14-microampere-hour bombardment where the ordinate represents the number of acceptable recoil tracks in each 100-kev interval in 0.0033 cc of the emulsion; (B) noise spectrum; and (C) the direct beam spectrum under the same conditions.

the scattering takes place isotropically. This is not justified in view of the continuum theory of nuclear reactions,³ but the deviation will reduce the signal and the noise in a similar manner. Figure 2 gives the results of the calculation of points (1) and (2) in reference to the geometry of Fig. 1 for a 14-microampere-hour bombardment of D-D neutrons from a half-atmosphere source of deuterium gas. The neutron energy in the forward-direction was taken to be 4.0 Mev. This gives about 3.75 Mev for the energy of the neutrons scattered from the ring into the emulsion. The background curve is a superposition of proton recoil spectra derived from the attenuated neutron flux scattered from the silver, bromine, oxygen, nitrogen, and carbon that are present in a 330-micron pellicle assumed to have the composition of an NTA emulsion.⁴ The actual spectra will be modified because of the following effects: spread in energy of the neutrons from the source; length of track projected onto the plane of the emulsion; range straggling in the emulsion. None of these effects are expected to destroy the general appearance of peaks.

An investigation of point (3) shows that the proton recoil spectrum between 4 Mev and 1-2 Mev is negligible. This estimate is based on measurement of the shadow cone background neutron flux as a function of neutron energy in our previous total scattering cross-section measurements.⁵

The signal-to-noise ratio for elastic scattering is seen to be large enough to make the experiment feasible. The inelastic scattering should be comparable with the elastic scattering and hence should be detected by this method. Preliminary measurements using an iron ring scatterer and 4-Mev neutrons show both the elastic and an inelastic group of neutrons separated by about 0.8 Mev in accordance with the expected excited level⁶ in Fe⁵⁶.

* Assisted by the joint program of the U. S. Office of Naval Research and the U. S. Atomic Energy Commission.

¹ H. T. Richards, Phys. Rev. 59, 796 (1941).

² F. Ajzenberg and T. Lauritsen, Revs. Modern Phys. 24, 321 (1952).

³ Final Report of the Fast Neutron Data Project NYO-636.

⁴ A. Beiser, Revs. Modern Phys. 24, 273 (1952).

⁵ S. C. Snowdon and W. D. Whitehead, Phys. Rev. 90, 615 (1953).

⁶ Nuclear Data, Natl. Bur. Standards (U. S.) Circular 499 (1950).

Nuclear Emulsion Method for Energy Measurement of Inelastically Scattered Neutrons*

S. C. SNOWDON, M. A. ROTHMAN, D. W. KENT, JR.,
AND W. D. WHITEHEAD

Bartol Research Foundation of The Franklin Institute,
Swarthmore, Pennsylvania

(Received April 1, 1953)

NUCLEAR emulsions have been used for some time in what may be called a point source of neutron geometry (point geometry) to record the energy spectrum of neutrons produced in nuclear reactions. The same method applied to the observation of inelastically-scattered neutrons has two defects: (a) the source of bombarding particles is relatively weak because these particles first must be produced by a nuclear reaction in order to get monoenergetic neutrons; (b) the bombarding neutrons as well as the scattered neutrons give proton recoils in the emulsion. The purpose of this letter is to present a method of overcoming these defects. Since the low intensity of flux incident on the scatterer cannot be increased appreciably, one can only hope to arrange the scatterer geometry so that many scattering points give similar contributions to the proton recoil spectrum. In order to prevent the direct neutron flux from producing a proton recoil spectrum comparable with that from the scatterer, it is necessary that the plane of the emulsion be placed at right angles to the incident flux. Both of these conditions are met if the scattering material is placed in an axially symmetric ring (ring geometry), and the photographic emulsion is located on the axis with its plane in the central plane of the ring (Fig. 1).

In order to utilize the ring geometry, the customary acceptance criteria¹ must be changed to the following single criterion: all proton recoil tracks are acceptable if their angle of dip with respect to the plane of the emulsion is less than θ_0 . In our case $\theta_0 = 12^\circ$. The feasibility of the ring geometry will have been ascertained if a calculation is made of the recoil proton spectrum from the following sources of scattered neutrons: (1) the ring (signal); (2) all elements in the emulsion (noise); and (3) the boundaries of the room (noise).

It should be noted that the noise of type (2) may be reduced by interposing some scattering material on the axis between the neutron source and the emulsion. Also, there will be a proton spectrum in the emulsion because of the $N^{14}(n, p)$ reaction ($Q = 0.627$ Mev).² This spectrum may easily be distinguished from the scattering spectrum, first because it will have a line spectrum, and secondly, because of the positive Q value, the peak will occur at an energy appreciably higher than that of the scattered neutron spectra.

In order to investigate points (1) and (2), it will be assumed that

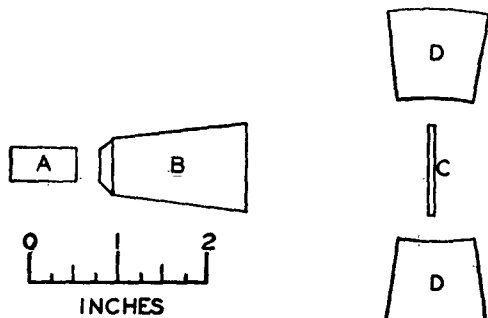


FIG. 1. Ring geometry for scatterer: (A) deuterium gas at one-half atmosphere pressure to give neutrons of 4 Mev from the D-D reaction; (B) copper shield that attenuates the direct neutron flux on the emulsion by $1/e$; (C) 330-micron NTA pellicle of about one inch diameter; (D) scatterer 6 inch i.d., 8 inch o.d., 12° half-angle from center of emulsion.

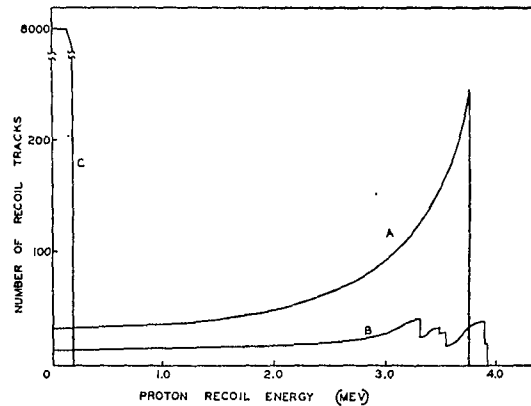


FIG. 2. Proton recoil spectra: (A) Signal spectrum of neutrons elastically scattered from iron for a 14-microampere-hour bombardment where the ordinate represents the number of acceptable recoil tracks in each 100-kev interval in 0.0033 cc of the emulsion; (B) noise spectrum; and (C) the direct beam spectrum under the same conditions.

the scattering takes place isotropically. This is not justified in view of the continuum theory of nuclear reactions,³ but the deviation will reduce the signal and the noise in a similar manner. Figure 2 gives the results of the calculation of points (1) and (2) in reference to the geometry of Fig. 1 for a 14-microampere-hour bombardment of D-D neutrons from a half-atmosphere source of deuterium gas. The neutron energy in the forward-direction was taken to be 4.0 Mev. This gives about 3.75 Mev for the energy of the neutrons scattered from the ring into the emulsion. The background curve is a superposition of proton recoil spectra derived from the attenuated neutron flux scattered from the silver, bromine, oxygen, nitrogen, and carbon that are present in a 330-micron pellicle assumed to have the composition of an NTA emulsion.⁴ The actual spectra will be modified because of the following effects: spread in energy of the neutrons from the source; length of track projected onto the plane of the emulsion; range straggling in the emulsion. None of these effects are expected to destroy the general appearance of peaks.

An investigation of point (3) shows that the proton recoil spectrum between 4 Mev and 1-2 Mev is negligible. This estimate is based on a measurement of the shadow cone background neutron flux as a function of neutron energy in our previous total scattering cross-section measurements.⁵

The signal-to-noise ratio for elastic scattering is seen to be large enough to make the experiment feasible. The inelastic scattering should be comparable with the elastic scattering and hence should be detected by this method. Preliminary measurements using an iron ring scatterer and 4-Mev neutrons show both the elastic and an inelastic group of neutrons separated by about 0.8 Mev in accordance with the expected excited level⁶ in Fe⁵⁶.

* Assisted by the joint program of the U. S. Office of Naval Research and the U. S. Atomic Energy Commission.

¹ H. T. Richards, Phys. Rev. 59, 796 (1941).

² F. Ajzenberg and T. Lauritsen, Revs. Modern Phys. 24, 321 (1952).

³ Final Report of the Fast Neutron Data Project NYO-636.

⁴ A. Beiser, Revs. Modern Phys. 24, 273 (1952).

⁵ S. C. Snowdon and W. D. Whitehead, Phys. Rev. 90, 615 (1953).

⁶ Nuclear Data, Natl. Bur. Standards (U. S.) Circular 499 (1950).

Angular Distribution of Neutrons Scattered from Aluminum, Iron, and Lead*

W. D. WHITEHEAD AND S. C. SNOWDON
Bartol Research Foundation of the Franklin Institute, Swarthmore, Pennsylvania
(Received May 29, 1953)

The differential cross sections for the scattering of 3.7-Mev neutrons from aluminum, iron, and lead have been measured in a ring geometry using a molded Lucite-zinc sulfide button as a detector. The measurements were taken over an angular range of 127 degrees between 13 degrees and 140 degrees with an angular resolution better than ± 10 degrees. Effects due to higher-order scattering in the scatterer were removed by extrapolation.

INTRODUCTION

M EASUREMENTS of the angular distribution of fast neutrons scattered from a large number of elements have been reported previously by Kikuchi *et al.*,¹ and Amaldi *et al.*,² in which the main features of the distribution could be explained as the diffraction effects due to the scattering of neutron waves by spherical particles. More recently Remund and Ricamo³ have measured angular distribution of 3.7-Mev neutrons scattered from carbon while Walt and Barschall,⁴ using 1.00-Mev neutrons have reported the angular distributions for a large number of elements. Feshbach, Porter, and Weisskopf,⁵ using a modification of the continuum theory of nuclear reactions, have reproduced the average features of the total neutron cross section *vs* energy and atomic number as measured by Barschall.⁶ Feshbach, Porter, and Weisskopf⁷ have also computed the angular distributions of elastically scattered neutrons using this same modification of the continuum theory and the

general features agree rather well with the measurements of Walt and Barschall.⁴ Our measurements on aluminum, iron and lead, using 3.7-Mev neutrons, were undertaken with the thought that the angular distribution in this energy range would be of value in view of the present theoretical considerations.

EXPERIMENTAL

Figure 1 shows the experimental arrangement that was used to measure the angular distribution of neutrons scattered from aluminum, iron, and lead. The source of neutrons is a chamber of deuterium gas at 0.5 atmosphere and 2.0 cm-in depth bombarded with about 10 microamperes of 1.0-Mev deuterons which, after passing through the nickel foil and gas, have a mean energy of about 0.65 Mev. These neutrons are detected by a pressure molded Lucite-zinc sulfide button⁸ mounted directly on the face of an RCA 5819 photomultiplier. The direct beam is cut out by a suitably tapered 10-inch long, $1\frac{1}{8}$ -inch diameter iron cylinder. The scatterer was chosen to have the shape of a ring in order to increase as much as possible the number of scattered neutrons. The scattering angle θ is varied by moving the scattering rings laterally and by using rings of various sizes. For angles between 52° and 140°, 8-inch o.d. rings were used with a mean source-detector distance R_0 of 40 cm. For θ between 24° and 52°, 6-inch o.d. rings were used with R_0 equal to 60 cm. For the point at 13°, 4-in. o.d. rings were used with R_0 equal to 72 cm.

In order to discuss the measurements that must be made to arrive at the differential scattering cross section, it is convenient to define several quantities. For a given number of neutrons emitted by the neutron source, let N_S be the number of neutrons recorded by the detector with the scatterer and direct beam attenuator in place. Let N_B be the number of neutrons detected with the scatterer removed and let N_D be the number of neutrons recorded with the scatterer and attenuator removed. $N_S - N_B$ is the number of scattered neutrons recorded by the detector that originate in the source, and $N_D - N_B$ is the number of neutrons direct from the source that are recorded by the detector. Let

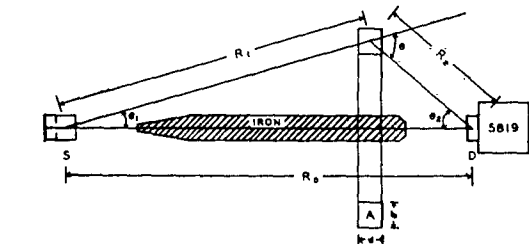


FIG. 1. Ring geometry for scatterer (S), deuterium gas at one-half atmosphere pressure to give neutrons of about 3.7 Mev; (D) Lucite-zinc sulfide scintillation detector; (A) ring scatterer of rectangular cross section.

* Assisted by the joint program of the U. S. Office of Naval Research and the U. S. Atomic Energy Commission.

¹ Kikuchi, Aoki, and Wakatuki, Proc. Phys. Math. Soc. Japan **21**, 410 (1939); T. Wakatuki and S. Kikuchi, Proc. Phys. Math. Soc. Japan **21**, 656 (1939); T. Wakatuki, Proc. Phys. Math. Soc. Japan **22**, 430 (1940).

² Amaldi, Bocciarelli, Cacciapuoti, and Trabacchi, International Conference on Fundamental Particles and Low Temperature (The Physical Society, London, 1947), Vol. 1.

³ A. E. Remund and R. Ricamo, Helv. Phys. Acta **25**, 441 (1952).

⁴ M. Walt and H. H. Barschall, Phys. Rev. **90**, 714 (1953).

⁵ Feshbach, Porter, and Weisskopf, Phys. Rev. **90**, 166 (1953).

⁶ H. H. Barschall, Phys. Rev. **86**, 431 (1952); Miller, Adair, Bockelman, and Darden, Phys. Rev. **88**, 83 (1952).

⁷ Feshbach, Porter, and Weisskopf, Bull. Am. Phys. Soc. **28**, No. 3, 29 (1953).

⁸ W. F. Hornyak, Rev. Sci. Instr. **23**, 264 (1952). The authors are indebted to Dr. Hornyak for supplying them with a Lucite-zinc sulfide molded button.

the scattering ratio be defined as

$$S = (N_S - N_B) / (N_D - N_B).$$

Appendix I then shows that the scattering ratio S is related to the apparent differential scattering cross section $\bar{\sigma}(\theta)$ through the relation

$$S = [I(\theta_1)/I(0)] \cdot [R_0^2/R_1^2 R_2^2] \cdot \bar{\sigma}(\theta) A(\theta_2) E(E_n) nV F(\theta_2) \exp(-\sigma nd), \quad (1)$$

where $I(\theta_1)$ is the number of neutrons emitted from the source per steradian per unit monitor flux, $A(\theta_2)$ is the angular sensitivity of the neutron detector normalized to unity at zero angle, $E(E_n)$ is the energy sensitivity of the neutron detector normalized to unity for the energy of the direct beam, nV is the number of scattering nuclei, σ is the total scattering cross section, and $F(\theta_2)$ is an attenuation factor which is defined more fully in Appendix I.

In general, the scattering ratio S is made up of a sum of terms $S = S_1 + S_2 + \text{etc.}$, where S_1 , S_2 , etc. refer to the neutrons scattered into the detector by single scattering, double scattering, etc. Thus, $\bar{\sigma}(\theta)$ is simply a measure of the differential scattering cross section, assuming that all neutrons are singly scattered, since $\bar{\sigma}(\theta)$ becomes exactly $\sigma(\theta)$ if S is replaced by S_1 . In order to separate the components S_1 , S_2 , etc., one measures the scattering ratio S for a fixed angle θ as a function of the axial thickness of the ring scatterer d . The value of $\sigma(\theta)$ at $d=0$ is then the average differential scattering cross section for all scattered neutrons (elastic and inelastic) weighted according to the energy-sensitivity of the detector $E(E_n)$. In the ideal case, if the energy-sensitivity curve adequately discriminates against the inelastically scattered neutrons, the above value of $\bar{\sigma}(\theta)$ for $d=0$ becomes the differential cross section for elastic scattering $\sigma(\theta)$.

In order to measure $\bar{\sigma}(\theta)$ it is necessary to consider the following factors.

1. *Energy resolution of incident neutrons.*—The mean energy of the neutrons incident on the scatterer varies between 3.70 Mev and 3.74 Mev depending on the angle θ_1 . The energy spread in the beam due to target thickness and voltage stability of the generator is about 200 kev.

2. *Neutron flux monitor.*—A proportional counter filled with one atmosphere of butane was placed very close to the target chamber at 90 degrees with respect to the source-detector axis. The discriminator was set to reject those neutrons that were produced from the $C^{12}(d, n)$ reaction in the vicinity of the magnet box. Actually some difficulty was experienced in obtaining a constant direct-beam neutron count per unit monitor count after the target chamber was just filled with deuterium. The pattern of change, however, was similar in each case and seemed to indicate that some of the deuterium gas was absorbed into the walls of the

chamber. After about an hour or two a ratio was obtained that was constant to ± 5 percent.

3. *Measurement of S .*—In general the direct beam count was about 15–100 times the scattered beam count and the attenuated direct beam count varied from 40 percent to 90 percent of the scattered beam count, each depending on the size and position of the scatterer.

4. *Spacial distribution of neutron source.*—The $N_D - N_B$ count exhibited within a few percent an inverse square variation with distance from the target chamber.

5. *Angular variation of the neutron flux from the D–D reaction, $I(\theta_1)/I(0)$.*—This quantity was computed from the data published by Hunter and Richards.⁹

6. *Measurement of nV , the number of scattering nuclei.*—Each scatterer was weighed on a suitable balance to about one percent accuracy.

7. *Angular variation in sensitivity of the neutron detector, $A(\theta_2)$.*—This quantity varied by about 25 percent over the range of θ_2 used in this experiment. The value of $A(\theta_2)$ was measured to within about 5 percent by rotating the detector about an axis through the detector perpendicular to the source-detector axis.

8. *Measurement of the total cross section.*—This was measured by using $1\frac{1}{2}$ -inch diameter, 1-inch long cylinders of aluminum, iron, and lead. The cross sections obtained for $E_n = 3.7$ Mev were $\sigma(\text{Al}) = 2.55$ barns, $\sigma(\text{Fe}) = 3.51$ barns, and $\sigma(\text{Pb}) = 7.60$ barns each in agreement with the values obtained by Nereson and Darden.¹⁰ The scattering-in corrections were 0.75, 2.4, and 4.3 percent, respectively, for Al, Fe, and Pb, and were obtained from our measurements of the differential cross section.

9. *The attenuation factor F .*—This factor varied from unity by as much as 14 percent depending on the size and shape of the scatterer. This quantity is discussed briefly in Appendix I and a graph of its variation is given in Fig. 2.

10. *Geometrical measurements.*—Measurements of distance were carried out to about ± 1 millimeter. The consequent calculation of mean angles is thus accurate to about one percent. However, because of the finite size of the detector (1 inch diameter, $\frac{1}{8}$ inch height) and the finite size of the scatterers, the detected neutrons are received over a range of angles of about ± 10 degrees in the worst case near $\theta = 90$ degrees.

11. *Variation of the sensitivity of the detector with neutron energy.*—This was measured by comparing our measurement of the angular distribution of neutrons from the D–D reaction with those of Hunter and Richards,⁹ the discrepancy being ascribed to a non-uniform efficiency in our detector. As may be seen in Fig. 3, the sensitivity only drops off slowly with decreasing neutron energy, decreasing by 40 percent in 1 Mev. Since it is desired to discriminate against neutrons that have lost more than 200 kev, this consti-

⁹ G. T. Hunter and H. T. Richards, Phys. Rev. 76, 1445 (1949).

¹⁰ N. Nereson and S. Darden, Phys. Rev. 89, 775 (1953).

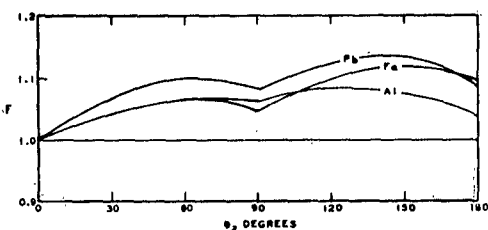


FIG. 2. Attenuation factor F . This quantity is defined in Appendix I. $F \exp(-\sigma d)$ essentially measures the attenuation of the direct beam into the scatterer times the attenuation of the scattered beam out of the scatterer. The dimensions are for aluminum, iron, and lead; $b = 2.54$ cm, 2.54 cm, and 2.54 cm; $d = 3.15$ cm, 2.54 cm, and 3.00 cm. The factor F is not shown for the thinner rings used in the experiment.

tutes a serious objection to the use of the Lucite-zinc sulfide detector in this experiment. However, if the inelastically scattered neutrons are more uniformly distributed in angle than the elastically scattered neutrons, then the general features of the differential cross section for elastic scattering will still be evident. In any case the value obtained for $\sigma(\theta)$ must be such that the total cross section achieved by integrating $\sigma(\theta)$ is less than the measured total cross section. That this is the case will be shown later.

12. *Sensitivity of counter to gamma rays.*—Neutron detector must not count the gamma rays resulting from the inelastic scattering of neutrons. An ampoule containing 0.1 milligram of radium was placed directly on the Lucite-zinc sulfide detector and gave a negligible counting rate (less than 1 count in 100 seconds).

13. *Higher-order scattering.*—Appendix II gives an account of the method used in this experiment to allow for double scattering. Essentially it involves placing an upper and lower bound on the possible values of $\bar{\sigma}(\theta)$ for an observed sequence of values of $\bar{\sigma}(\theta)$ as a function of the axial thickness of the ring. The first calculation estimates the nature of the variation of $\bar{\sigma}(\theta)$ with d/a under the assumption of isotropic scattering. This is given by Eq. (13) which, after comparing with Fig. 4, is

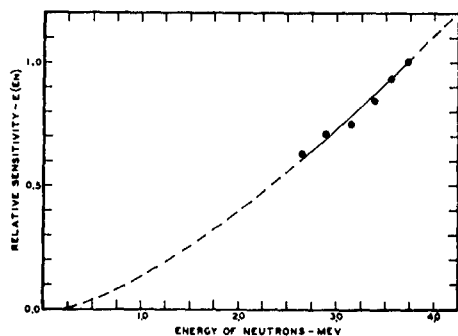


FIG. 3. Energy sensitivity of neutron detector. $E(E_n)$ measures the sensitivity of the neutron detector normalized to unity at 3.7 Mev. Solid circles were measured by us. The dotted curve was obtained from reference 9 by normalizing the two sets of data over the region common to both.

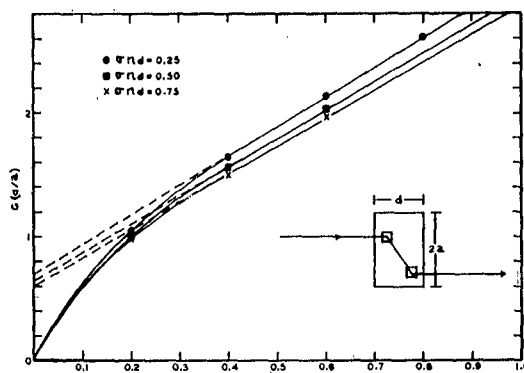


FIG. 4. Variation of straight-through double scattering in a right circular cylinder. The differential cross section was assumed to be isotropic. Specifically this curve is a plot of the function G as defined in Appendix II.

seen to reduce to the practical formula

$$\bar{\sigma}(\theta) = \bar{\sigma}_0(\theta) - 0.282\bar{\sigma}'(\theta), \quad (2)$$

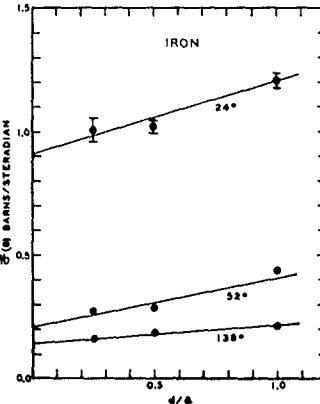
where $\bar{\sigma}_0(\theta)$ is the intercept at $d/a=0$ of the linear portion of the curve and $\bar{\sigma}'(\theta)$ is the slope of the $\bar{\sigma}(\theta)$ vs d/a curve in the linear portion.

The second calculation states that, if the angular distribution is peaked strongly forward, then one expects that the double scattering contribution will cause $\bar{\sigma}(\theta)$ to be a linear function of d or d/a . In this case $\bar{\sigma}_0(\theta)$ is the true differential scattering cross section. Both of these extrapolations are presented on the graphs.

If triple scattering is present, then $\bar{\sigma}(\theta)$ should be a quadratic function of d or d/a for the case in which there is a strong forward peaking of the scattering. Figure 5, for the case of iron, shows some indication of the presence of triple scattering; however, the experimental uncertainty is too large to consider this definite. No attempt was made to remove the triple scattering contributions.

A typical run of data was made as follows: (1) direct beam; (2) attenuated beam; (3) scattered beam from one of the rings for all values of the scattering angle; (4) attenuated beam; (5) direct beam. If the two

FIG. 5. Apparent differential cross section of iron vs thickness of ring scatterer for three different scattering angles. The thickness is measured relative to a quantity a , which we have taken to be equal to the radial width of the ring in order to establish a correspondence between the ring scatterer and the right circular cylinder scatterer.



NEUTRONS SCATTERED FROM Al, Fe, AND Pb

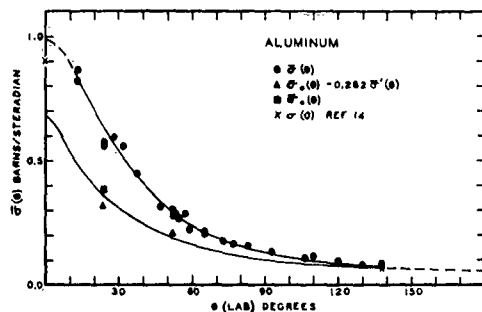


FIG. 6. Angular distribution of 3.7-Mev neutrons scattered from aluminum. $\hat{\sigma}(\theta)$ is apparent differential cross section as defined in the text. $\hat{\sigma}_0(\theta)$ is the differential cross section using a linear extrapolation to remove higher-order scatters. $\hat{\sigma}_0(\theta) - 0.282\sigma'(\theta)$ is the differential cross section in which the higher-order scatters are removed using the isotropic scattering assumption. $\sigma(0)$ is taken from the "Final Report of the Fast Neutron Data Project," U. S. Atomic Energy Commission, NYO-636 (unpublished), in which the nuclear radii were found from our measured values of the total cross section.

values of the direct beam determination differed by more than 10 percent, the data were discarded.

DATA

Figures 6-8 show the experimental points of the apparent differential cross section for 3.7-Mev neutrons incident on aluminum, iron, and lead as calculated from Eq. (1). Only a limited number of angles were chosen in order to determine the effects of higher-order scattering. Figure 5 shows the variation of $\hat{\sigma}(\theta)$ as a function of the ring thickness for the case of iron. In the same manner, similar curves were obtained for lead and aluminum. The extrapolations both for isotropic scattering and forward peaked scattering are shown in Figs. 6, 7, and 8 where a curve is drawn through the points thought to be the appropriate differential cross section, $\sigma(\theta)$ for each case. The total cross sections corresponding to $\sigma(\theta)$ have been calculated and are presented together with the previously measured total cross sections¹⁰ in Table I. It will be noted that the

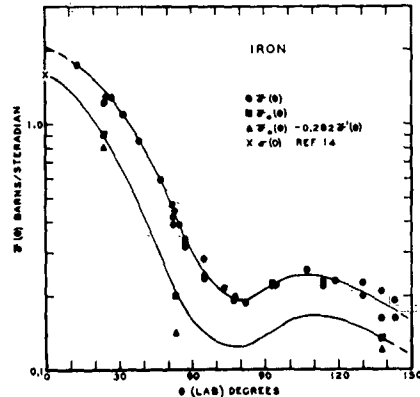


FIG. 7. Angular distribution of 3.7-Mev neutrons scattered from iron. Other remarks in caption of Fig. 6 apply here also.

TABLE I. Total cross sections. Subject to the reservations in the text, the value of $\int \sigma(\theta) d\Omega_\theta$ is the total elastic cross section.

Element	$\sigma_{\text{tot}} (\text{meas.})$ in barns This expt.	σ_{tot} in barns Ref. 10	$\int \sigma(\theta) d\Omega_\theta$ (barns)
Aluminum	2.55	2.50	1.73
Iron	3.51	3.55	2.94
Pb	7.60	7.70	5.17

integrated differential cross sections in each case are less than the measured total cross section. The total inelastic cross section cannot be obtained as the difference between the two former cross sections since the measurement of the differential cross section did not discriminate adequately against the inelastically scattered neutrons. However, this subtraction can be carried out approximately if one accepts the following rather crude estimate of the inelastic contribution to $\sigma(\theta)$. There are seven levels in aluminum that can be excited by 3.7-Mev neutrons.¹¹ If we assume that the maximum total inelastic cross section is about 50 percent of the total cross section and that the seven levels in aluminum are equally excited, then the inelastic neutrons contribute less than 15 percent to the total cross sections corresponding to $\sigma(\theta)$. Similar arguments using the known levels in iron and lead show that the inelastic contribution in these elements is less than 20 percent.

In conclusion, the authors wish to express their appreciation to Dr. W. F. G. Swann, Director of The Bartol Research Foundation, for his sustained interest in this problem.

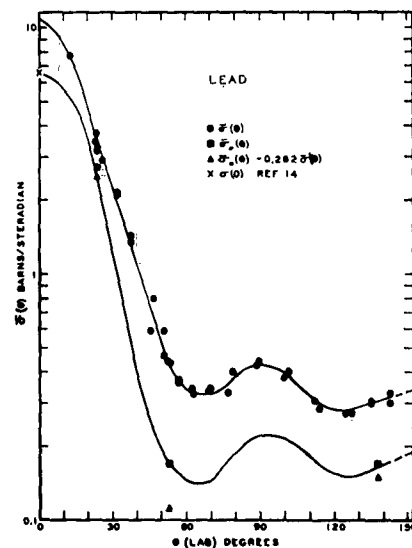


FIG. 8. Angular distribution of 3.7-Mev neutrons scattered from lead. Other remarks in caption of Fig. 6 apply here also.

¹¹ Nuclear Data, Natl. Bureau Standards Circ. 499 (U. S. Government Printing Office, Washington, D. C., 1950).

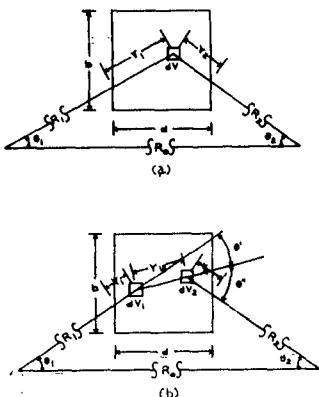


FIG. 9. Detail of scattering geometry:
(a) single scattering;
(b) double scattering.

APPENDIX I. SCATTERING OF NEUTRONS THROUGH RING SCATTERER BY SINGLE SCATTERING

In general the scattering ratio is made up of a sum of terms $S = S_1 + S_2 + \dots$, where S_1, S_2 , etc., refer to the neutrons scattered into the detector by single scattering, double scattering, etc. For the single scattering case [Figs. 1 and 9(a)] we have

$$S_1 = \int_V [I(\theta_1)/I(0)] \cdot [R_0^2/R_1^2 R_2^2] \cdot \sigma(\theta) n \times \exp[-\sigma n(r_1+r_2)] \cdot A(\theta_2) E(E_n) dV. \quad (3)$$

The geometry is such that only small errors will be introduced if Eq. (3) is replaced by

$$S_1 = [I(\theta_1)/I(0)] \cdot [R_0^2/R_1^2 R_2^2] \cdot \sigma(\theta) n A(\theta_2) E(E_n) V F(\theta_2) \exp(-\sigma n d), \quad (4)$$

where

$$F = V^{-1} \int_V \exp[-\sigma n(r_1+r_2-d)] dV, \quad (5)$$

and the mean angles and distances are used for $\theta_1, \theta_2, R_0, R_1$, and R_2 . For a fixed size of ring scatterer, the quantity F is a function of θ_1 and θ_2 . However, since θ_1 only varies from about 5° to 15° , little error and much simplification is introduced by computing F for $\theta_1=0$. For the rectangular cross section of our scatterer, the integral F may be evaluated in terms of elementary functions. The results are displayed in Fig. 2.

If only single scattering were present, the quantity S_1 could be replaced by the measured data S and the differential cross section $\sigma(\theta)$ could be calculated. In any case the reduction of the data is facilitated by defining an effective single scattering differential cross section $\delta(\theta)$ such that

$$S = [I(\theta_1)/I(0)] \cdot [R_0^2/R_1^2 R_2^2] \cdot \delta(\theta) n A(\theta_2) E(E_n) V F(\theta_2) \exp(-\sigma n d). \quad (6)$$

APPENDIX II. SCATTERING OF NEUTRONS THROUGH RING SCATTERER BY DOUBLE SCATTERING

Using the quantities defined in Figs. 1 and 9b, the double scattering ratio is seen to be

$$S_2 = \int_{V_1} \int_{V_2} [I(\theta_1)/I(0)] \cdot [R_0^2/R_1^2 r_{12}^2 R_2^2] \cdot \sigma(\theta') \sigma(\theta'') n^2 \exp[-\sigma n(r_1+r_{12}+r_2)] \times A(\theta_2) E(E_n) dV_1 dV_2. \quad (7)$$

An analytical solution of this integral seems quite involved, if not hopeless, for the geometry of the ring scatterer. In order to get some feeling for the manner in which the double scattering varies with the thickness of the ring, we have chosen to calculate the straight-through double scattering from a right circular cylinder assuming isotropic scattering [$\sigma(\theta')=\text{const}=\sigma/4\pi$]. In order to simplify this case as much as possible, let the neutron beam, incident on the circular end of the cylinder, be parallel to the cylinder axis, and let the detector sensitivities $A(\theta_2)=E(E_n)=1$. Also let r_1+r_2 be replaced by an approximate mean value d , the thickness of the cylinder. Equation (7) then reduces to

$$S_2 = [\sigma^2 n^2 / 16\pi^2 R_2^2] \cdot \exp(-\sigma n d) \times \int_{V_1} \int_{V_2} r_{12}^{-2} \exp(-\sigma n r_{12}) dV_1 dV_2. \quad (8)$$

If the exponential function is expanded and the first three terms retained, S_2 reduces to the following:

$$S_2 = [\sigma^2 n^2 a^4 / 16 R_2^2] \cdot \exp(-\sigma n d) \cdot (X - \sigma n a Y + \frac{1}{2} \sigma^2 n^2 a^2 Z), \quad (9)$$

where

$$X = -2(d^2/a^2) \cdot \ln d/a + 2(d^2/a^2) \sinh^{-1} d/2a + \cosh^{-1}(1+d^2/2a^2) + 2d^2/a^2 - d^4/4a^4 - (1-d^2/2a^2) \cdot [(1+d^2/2a^2)^2 - 1]^{\frac{1}{2}}, \quad (10)$$

$$Y = 8 \int_0^\infty [xd/2a - \exp(-xd/2a)] \times \sinh(xd/2a) J_1(x) \sin x \cdot dx/x^4, \quad (11)$$

and

$$Z = d^2/a^2. \quad (12)$$

The integration of X was facilitated by the use of a theorem in vector analysis.¹² The integration of Y can be effected by recognizing that the integral corresponds to the electrostatic energy of a uniform volume distribution of charge.¹³

If the single scattering ratio S is calculated for the right circular cylinder under the same assumptions, then

¹² H. B. Phillips, *Vector Analysis* (John Wiley and Sons, Inc., New York, 1933), Chap. III.

¹³ W. R. Smythe, *Static and Dynamic Electricity* (McGraw-Hill Book Company, Inc., New York, 1939), Chap. V.

the effective single scattering cross section is given by

$$\frac{\dot{\sigma}}{\sigma} = 1 + (\sigma n a / 4) G(d/a), \quad (13)$$

where

$$G(d/a) = (a/d)(X - \sigma n a Y + \frac{1}{2} \sigma^2 n^2 a^2 Z) \quad (14)$$

and is written only as a function of d/a since it varies but slowly with $\sigma n a$, as may be seen in Fig. 4. By considering the mean curve to apply to all cases of interest, the function G becomes a function of d/a only.

To apply the calculations of the right circular cylinder to the case of the ring scatterer, we assume that except for multiplying factors which are angular functions,

the geometrical variation of the single and double scattering ratios is given correctly after associating the radial thickness of the ring scatterer b with the radius of the cylinder a .

If, instead of isotropic scattering, one takes the other extreme of an angular distribution peaked strongly in the forward direction, one finds that the single scattering ratio in the ring scattering varies as $d \exp(-\sigma n d)$ whereas the double scattering ratio varies as $d^2 \exp(-\sigma n d)$; thus leading to a linear variation of the apparent single scattering cross section with the thickness of the ring.

Distribution List

Argonne National Laboratory, Attn: A. S. Langsdorf
P. O. Box 5207, Chicago 80, Illinois

Brookhaven National Laboratory, Attn: D. J. Hughes
Upton, Long Island, New York

Prof. H. Newson, Department of Physics, Duke University
Durham, North Carolina

E. I. DuPont de Nemours Co., Attn: C. W. J. Wende
Nemours Building, Wilmington 98, Delaware

Dr. G. E. Owen, Johns Hopkins University
Baltimore 18, Md.

Prof. J. D. Stranathan, Department of Physics
University of Kansas, Lawrence, Kansas

Dr. P. F. Gast, Hanford Works
P. O. Box 550, Richland, Washington

Knolls Atomic Power Laboratory, Attn: T. M. Snyder
P. O. Box 1072, Schenectady, New York

Los Alamos Scientific Laboratory, Attn: R. F. Taschek
P. O. Box 1663, Los Alamos, New Mexico

Dr. W. M. Preston, Laboratory for Nuclear Science and
Engineering, Massachusetts Institute of Technology,
Cambridge 39, Massachusetts

U. S. Atomic Energy Commission, Attn: R. F. Van Wye
Division of Technical Advisors, New York Operations Office
P. O. Box 30, Ansonia Station, New York 23, New York

North American Aviation, Inc., Attn: Chauncey Starr
P. O. Box 309, Downey, California

Oak Ridge National Laboratory, Attn: A. H. Snell
P. O. Box P, Oak Ridge, Tennessee

Prof. T. W. Bonner, Department of Physics
Rice Institute, Houston, Texas

Dr. J. W. Coltman, Research Laboratories
Westinghouse Electric Corporation
East Pittsburgh, Pennsylvania

Westinghouse Electric Corporation, Attn: S. Krasik
Atomic Power Division, Bettis Field, P. O. Box 1468
Pittsburgh 30, Pennsylvania

Prof. R. H. Herb, Department of Physics
University of Wisconsin, Madison 6, Wisconsin

Dr. J. L. McKibben, Los Alamos Scientific Laboratory
P. O. Box 1663, Los Alamos, New Mexico

Dr. R. A. Peck, Jr., Department of Physics
Brown University, Providence 12, Rhode Island

Chief of Naval Research, Attn: Nuclear Physics Branch
Navy Department, Washington 25, D. C.

Director
Office of Naval Research, Chicago Branch Office
844 North Rush Street, Chicago 11, Illinois

Director
Office of Naval Research, San Francisco Branch Office
801 Donahue Street, San Francisco 24, California

Director
Office of Naval Research, New York Branch Office
346 Broadway, New York 13, New York

Director
Office of Naval Research, Pasadena Branch Office
1030 E. Green Street, Pasadena 1, California

Officer in Charge
Office of Naval Research, London Branch Office,
Navy No. 100, Fleet Post Office, New York, New York

Dr. George A. Kolstad, Chief, Physics and Mathematics Branch
Division of Research, U. S. Atomic Energy Commission
Washington 25, D. C.

Superintendent, Nucleonics Division
Naval Research Laboratory, Anacostia, Washington, D. C.

Chief of the Bureau of Ships, Attn: Code 390
Navy Department, Washington 25, D. C.

Chief of the Bureau of Ships, Attn: Code 330
Navy Department, Washington 25, D. C.

Chief of the Bureau of Ordnance, Attn: Rem
Navy Department, Washington 25, D. C.

Chief of the Bureau of Ordnance, Attn: Re9a
Navy Department, Washington 25, D. C.

Chief of the Bureau of Aeronautics,
Attn: Applied Nuclear and General Physics Branch
Navy Department, Washington 25, D. C.

Officer in Charge, Naval Radiological Defense Laboratory
San Francisco Naval Shipyard, San Francisco, California

Chief of Naval Operations, Attn: Op 36
Navy Department, Washington 25, D. C.

Senior Scientific Advisor
Office of the Under Secretary of the Army
Department of the Army, Washington 25, D. C.

Director, Research and Development Division
General Staff
Department of the Army, Washington 25, D. C.

National Bureau of Standards Library
Room 203, Northwest Building, Washington 25, D. C.

Commanding General
Air Research and Development Command, Attn: RDRRP
P. O. Box 1395, Baltimore 3, Md.

Nuclear Development Associates, Inc., Attn: Dr. H. Goldstein
80 Grand Street, White Plains, New York

Dr. V. L. Parsegian
Director, Research Division
U. S. Atomic Energy Commission, New York Operations Office
P. O. Box 30, Ansonia Station, New York 23, New York